

# Counterflow and wall stagnation flow with three-dimensional strain

Cite as: Phys. Fluids **31**, 053605 (2019); <https://doi.org/10.1063/1.5096472>

Submitted: 18 March 2019 . Accepted: 08 May 2019 . Published Online: 31 May 2019

William A. Sirignano



View Online



Export Citation



CrossMark

## ARTICLES YOU MAY BE INTERESTED IN

[Kinetic modeling of unsteady hypersonic flows over a tick geometry](#)

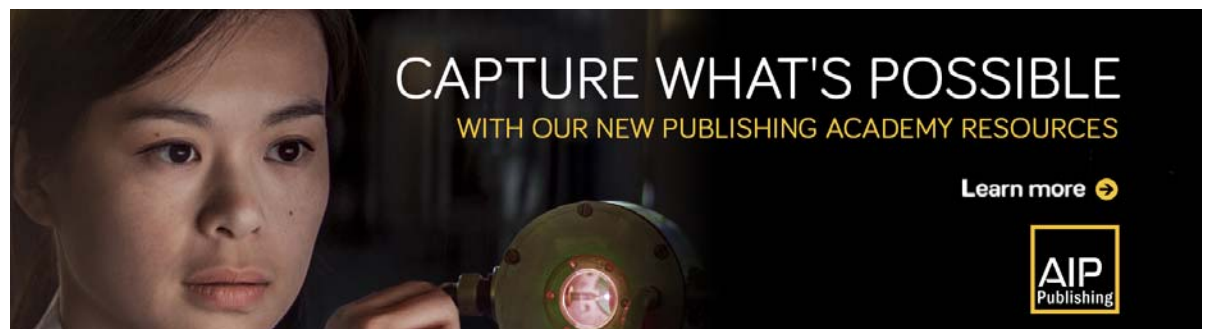
Physics of Fluids **31**, 056108 (2019); <https://doi.org/10.1063/1.5090341>

[Dispersion due to combined pressure-driven and electro-osmotic flows in a channel surrounded by a permeable porous medium](#)

Physics of Fluids **31**, 056603 (2019); <https://doi.org/10.1063/1.5092199>


[Stokes-layer formation under absence of moving parts—A novel oscillatory plasma actuator design for turbulent drag reduction](#)

Physics of Fluids **31**, 051701 (2019); <https://doi.org/10.1063/1.5094388>



CAPTURE WHAT'S POSSIBLE  
WITH OUR NEW PUBLISHING ACADEMY RESOURCES

Learn more →



# Counterflow and wall stagnation flow with three-dimensional strain

Cite as: Phys. Fluids 31, 053605 (2019); doi: 10.1063/1.5096472

Submitted: 18 March 2019 • Accepted: 8 May 2019 •

Published Online: 31 May 2019



View Online



Export Citation



CrossMark

William A. Sirignano<sup>a)</sup>

## AFFILIATIONS

Department of Mechanical and Aerospace Engineering University of California, Irvine, California 92697, USA

<sup>a)</sup>sirignan@uci.edu

## ABSTRACT

Three-dimensional (3D) viscous counterflows and wall stagnation flows are analyzed with differing normal strain rates in each of the three directions. Reduction of the equations to a similar form is obtained allowing for variations in density due to temperature and composition, heat conduction, and, for the counterflow, mass diffusion and the presence of a flame. Solutions to the Navier-Stokes equations are obtained without the boundary-layer approximation. For the steady and unsteady incompressible counterflows, analytical solutions are obtained for the flow field and the scalar fields subject to heat and mass transfer. In steady, variable-density configurations, a set of ordinary differential equations (ODEs) governs the two transverse velocity and the axial velocity profiles as well as the scalar-field variables. Diffusion rates for mass, momentum, and energy depend on the two normal strain rates parallel to the counterflow interface or the wall and thereby not merely on the sum of those two strain rates. For thin diffusion flames, the location, burning rate, and peak temperature are readily obtained. Solutions for planar flows and axisymmetric flows are obtained as limits here. Results for the velocity and scalar fields are found for a full range of the distribution of normal strain rates between the two transverse directions, various Prandtl number values, and various ambient (or wall) temperatures. For counterflows with flames and stagnation layers with hot walls, velocity overshoots are seen in the viscous layer, yielding an important correction of theories based on a constant-density assumption.

Published under license by AIP Publishing. <https://doi.org/10.1063/1.5096472>

## NOMENCLATURE

$c_p$	specific heat under constant pressure [J/(K kg)]
$D$	mass diffusivity ( $\text{m}^2/\text{s}$ )
$H$	specific enthalpy defined before Eq. (6) (J/kg)
$\tilde{H} = h + (u^2 + v^2 + w^2)/2 \approx h + v^2/2$	alternative specific enthalpy (J/kg)
$h$	specific enthalpy (J/kg)
$h_{f,m}$	heat of formation for species (mJ/kg)
$Le = \lambda / (c_p \rho D)$	Lewis number
$M$	Mach number
$N$	number of species
$p$	pressure ( $\text{N}/\text{m}^2$ )
$Pr$	Prandtl number
$R$	specific gas constant [J/(K kg)]
$R_u$	universal gas constant [J/(K mole)]
$S_1$	normal strain rate in the $x$ direction ( $\text{s}^{-1}$ )
$S_2$	normal strain rate in the $z$ direction ( $\text{s}^{-1}$ )
$t$	time (s)
$u, v, w$	velocity components (m/s)
$x, y, z$	Cartesian coordinate (m)

$Y_m$	mixture fraction
$Z$	mass fraction of species
$\alpha, \beta$	conserved scalars
$\eta$	density weighted coordinate ( $\text{kg}/\text{m}^2$ )
$\lambda$	thermal conductivity [J/(sm <sup>2</sup> )]
$\rho$	density ( $\text{kg}/\text{m}^3$ )
$\dot{\omega}_m$	reaction rate for species ( $\text{s}^{-1}$ )
$\tau_{ij}$	viscous stress tensor ( $\text{N}/\text{m}^2$ )

## Superscripts

*	dimensional values
'	ordinary derivative

## Subscripts

$i, j, k$	integers for vector and tensor component designation
$m$	integer for species designation
$w$	conditions at the wall or relevant to the stagnation wall flow
$\infty$	conditions at positive infinite $y$
$-\infty$	conditions at negative infinite $y$

## I. INTRODUCTION

Here, we treat a three-dimensional (3D) counterflow with differing strain rates in each direction. It can address counterflows in nonsymmetric fields or wall stagnation flows for nonsymmetric aerodynamic bodies. Two counterflowing streams might be constrained to have greater acceleration in one transverse direction than in the other. The aerodynamic body at the stagnation point might have differing radii of curvature in two mutually orthogonal planes which are each orthogonal to the tangent plane at that stagnation point.

There is growing interest in understanding the laminar mixing and combustion that commonly occurs within turbulent eddies. These laminar subdomains experience significant strain. Some important work has been done here but typically in two-dimensions or axisymmetry with a constant-density approximation. See the work of Linan,<sup>1</sup> Marble,<sup>2</sup> Karagozian and Marble,<sup>3</sup> Cetegen and Sirignano,<sup>4,5</sup> and Peters.<sup>6</sup> Karagozian and Marble did examine a three-dimensional strained-flow configuration where flow moved radially inward and jetted axially outward; in addition, a vortex had the same axis as the flow. The vortex caused the diffusion flame sheet to wrap around the axis. Recently, Rajamanickam *et al.*<sup>7</sup> have provided an interesting three-dimensional triple-flame analysis; the imposed strain however is limited to two dimensions. There is a strong need to study mixing and combustion in counterflows where the imposed strain is three-dimensional. Note that Nguyen *et al.*<sup>8</sup> and Nguyen and Sirignano<sup>9</sup> have recently shown the importance of strained triple flames in practical combustors.

The “counterflow” label has been given to several types of distinct flows. One type involves two parallel, adjacent flows in opposite directions and possibly in different conduits. These flows are common in heat exchangers.<sup>10</sup> Another type of counterflow is actually a recirculating flow caused by an imposed swirl.<sup>11</sup> A third kind involves two mutually penetrating flows such as that found with a superfluid and normal fluid moving in opposite directions through the same volume.<sup>12</sup> The references above are merely samples; a thorough review of those types of counterflows is not intended. Here, we focus only on a fourth kind where two streams move toward each other in the  $y$  direction with velocities of opposite signs but then turn toward the  $x$  and  $z$  directions before they make contact with each other at an interface in a plane normal to the  $y$  direction.  $v$ , the  $y$  component of velocity, becomes zero at this interface.

There is a well-established literature for steady-state viscous two-dimensional and axisymmetric counterflows and stagnation-point flows.<sup>13</sup> Strahle<sup>14</sup> examined the axisymmetric, unsteady stagnation point, including the presence of heat and mass transport and a diffusion flame. However, three-dimensional viscous flows of these types have not received very much fundamental treatment. Howarth<sup>15</sup> has treated the steady, 3D wall stagnation-point flow for an incompressible fluid. Heat transfer was not considered there. Here, generalizations for variable-density viscous counterflows and wall-stagnation flows are presented for several basic configurations. Density variations through the flow due to variations in temperature, pressure, and/or composition are considered. Heat transfer caused by different temperature values between the two opposing streams or between the incoming stream and a wall is examined. Also, mass transfer for the counterflow caused by differing compositions of the two opposing streams is considered. A counterflow with a diffusion

flame is also considered. Still, there are some similarities between the approach here and the portions of Howarth’s analysis.

Substantial work has occurred for planar and axisymmetric counterflow diffusion flames with single-phase flows at moderate pressures.<sup>1,6,16–19</sup> The axisymmetric counterflow configuration has also been studied for spray combustion<sup>20,21</sup> and at supercritical pressures.<sup>22</sup> Here, an extension will be made for a three-dimensional counterflow at moderate pressures and a gaseous phase.

The prior counterflow and stagnation-point studies (cited above) address typically two-dimensional configurations (planar or axisymmetric). As an exception, Howarth addresses three-dimensional, incompressible wall flow. They obtain a similar solution whereby a system of ordinary differential equations (ODEs) with only one spatial coordinate remaining as the independent variable; the description of dependence on the other spatial coordinate(s) is given in algebraic terms. Our work here presents similar solutions for three-dimensional flows where again only one coordinate appears as the independent variable. The one-dimensional appearance of the final governing equations is not a model but still is an exact solution of a multidimensional configuration.

Aerodynamic studies of the shape of the interface between two counterflows have also been performed.<sup>23,24</sup> Here, a free-stream velocity and a radius of curvature of a counterflow-interface or a wall radius of curvature will not be specified. Rather, the order of magnitude of that ratio of velocity to radius is implied through the prescribed strain rate. The incoming counterflow streams will have a potential-flow character.

Here, we address a set of three-dimensional counterflows and stagnation-point flows, steady and unsteady, with and without combustion, and with and without constant density and properties. These various problems have differences but are not totally independent.

## II. ANALYSIS

Consider, for example, a counterflow from both the negative  $y$ -direction and positive  $y$ -direction with outflow in the  $z$ -directions. Inflow or outflow can occur in the  $x$ -direction with the interface surface along  $y = 0$  and a stagnation point at  $x = y = z = 0$ . The velocity  $\vec{u}$  has the components  $u$ ,  $v$ , and  $w$  in the  $x$ ,  $y$ , and  $z$  directions, respectively. The flow must have a negative normal strain rate in at least one direction; the  $y$ -direction has arbitrarily been chosen here to be the direction with the only negative strain rate. The  $z$ -direction has the larger positive (or equal) strain rate, while the  $x$ -direction has a smaller (or equal) normal strain rate. If the approaching streams have the same pressure at a distance from the interface and its viscous layer, we expect that in a frame of reference attached to the interface, momentum balance for steady flow yields  $\rho_{-\infty} v_{-\infty}^2 = \rho_{\infty} v_{\infty}^2$ . The incoming flow is in the direction of decreasing  $y$ -magnitude. The normal strain rates in the  $x$ - and  $z$ -directions are  $S_1 = \partial u / \partial x$  and  $S_2 = \partial w / \partial z$ , respectively. Here,  $S_1 + S_2 > 0$  and  $S_2 > 0$ .  $S_1$  can be positive or negative. These normal strain rates for these two opposing streams will match at the interface since the velocity components are continuous there. We are able to find a solution in the stagnation point region where these two strain rates apply throughout the viscous layer and do not vary with  $y$ . We consider only  $S_1 \geq 0$ , which is a classical counterflow

with the interface at  $y = 0$ . If  $S_1 < 0$ , there would be sink inflow in the  $x$ - and  $y$ -directions with outjetting in the  $z$ -direction. This case is not addressed by our similar-solution approach. The  $y$ -directed inflowing streams in all cases bring together fluids of differing temperature and/or composition; so, heat and mass diffusion are in the  $y$ -direction.

The two streams need not have the same upstream values for velocity  $v$ , temperature  $T$ , enthalpy  $h$ , density  $\rho$ , or composition reflected through mass fraction  $Y_m$  for chemical species  $m$ . Pressure  $p$  will be given the same upstream values for the two streams. Fickian mass diffusion and Fourier heat conduction are considered so that all fluid properties are continuous across the interface. Some consideration is given to reacting flows. Radiation and gravity are neglected. The formulation of the partial differential equations below will also apply for a stagnating flow approaching a wall at  $y = 0$ .

With the addition of terms accounting for chemical rates for exothermic reactions, diffusion flames can be addressed by the analysis here. With a variation in the boundary conditions, the analysis will apply to wall stagnation-point flows. There are several studies of planar and axisymmetric counterflow diffusion flames with account given to variable density;<sup>17-19</sup> no prior works on 3D strained diffusion flames are known.

The governing equations for unsteady 3D flow are given as

$$\frac{\partial \rho}{\partial t} + \frac{\partial(\rho u_j)}{\partial x_j} = 0, \tag{1}$$

$$\rho \frac{\partial u_i}{\partial t} + \rho u_j \frac{\partial u_i}{\partial x_j} + \frac{\partial p}{\partial x_i} = \frac{\partial \tau_{ij}}{\partial x_j}, \tag{2}$$

where, following the Stokes hypothesis for a Newtonian fluid,

$$\tau_{ij} = \mu \left[ \frac{\partial u_i}{\partial x_j} + \frac{\partial u_j}{\partial x_i} - \frac{2}{3} \delta_{ij} \frac{\partial u_k}{\partial x_k} \right], \tag{3}$$

$$\begin{aligned} \rho \frac{\partial h}{\partial t} + \rho u_j \frac{\partial h}{\partial x_j} - \frac{\partial p}{\partial t} - u_j \frac{\partial p}{\partial x_j} \\ = \frac{\partial}{\partial x_j} \left( \frac{\lambda}{c_p} \frac{\partial h}{\partial x_j} \right) + \frac{\partial}{\partial x_j} \left( \rho D (1 - Le) \sum_{m=1}^N h_m \frac{\partial Y_m}{\partial x_j} \right) \\ - \rho \sum_{m=1}^N h_{f,m} \dot{\omega}_m + \tau_{ij} \frac{\partial u_i}{\partial x_j}, \end{aligned} \tag{4}$$

$$\rho \frac{\partial Y_m}{\partial t} + \rho u_j \frac{\partial Y_m}{\partial x_j} = \frac{\partial}{\partial x_j} \left( \rho D \frac{\partial Y_m}{\partial x_j} \right) + \rho \dot{\omega}_m ; \quad m = 1, 2, \dots, N. \tag{5}$$

An alternative form of the energy equation can be developed to govern the total  $H$  of the specific enthalpy, specific chemical energy,

and kinetic energy per unit mass. That is,  $H \equiv h + \sum_{m=1}^N Y_m h_{f,m} + u_k u_k / 2$ . Specifically, the vector dot product of  $u_i$  with Eq. (2) is used to substitute for  $u_j \partial p / \partial x_j$  in Eqs. (4) and (5) is used to substitute for  $\dot{\omega}_m$  there. The Lewis number  $Le = 1$  is considered. It follows that

$$\rho \frac{\partial H}{\partial t} + \rho u_j \frac{\partial H}{\partial x_j} - \frac{\partial p}{\partial t} = \frac{\partial}{\partial x_j} \left( \frac{\lambda}{c_p} \frac{\partial (h + \sum_{m=1}^N Y_m h_{f,m})}{\partial x_j} \right) + \frac{\partial (u_i \tau_{ij})}{\partial x_j}. \tag{6}$$

The nondimensional forms of the above equations remain identical to the above forms if we choose certain reference values for normalization. In the remainder of this article, the nondimensional forms of the above equations will be considered. The superscript  $*$  will be used to designate a dimensional property. The variables  $u_i^*, t^*, x_i^*, \rho^*, h^*, p^*$ , and  $\dot{\omega}_m^*$  and properties  $\mu^*, \lambda^* / c_p^*$ , and  $D^*$  are normalized, respectively, by  $[(S_1^* + S_2^*) \mu_\infty^* / \rho_\infty^*]^{1/2}, (S_1^* + S_2^*)^{-1}, [\mu_\infty^* / (\rho_\infty^* (S_1^* + S_2^*))]^{1/2}, \rho_\infty^*, (S_1^* + S_2^*) \mu_\infty^* / \rho_\infty^*, (S_1^* + S_2^*) \mu_\infty^*, \mu_\infty^*, \mu_\infty^*$ , and  $\mu_\infty^* / \rho_\infty^*$ . It is understood that for unsteady flow, the reference values for strain rates and far-stream variables and properties used for normalization will be constants; for example, averages might be taken for fluctuating conditions. Note that the reference length  $[\mu_\infty^* / (\rho_\infty^* (S_1^* + S_2^*))]^{1/2}$  is the estimate for the magnitude of the viscous-layer thickness.

The stagnation point either in the steady counterflow or in the steady flow against a wall will be taken as the origin  $x = y = z = 0$ . Along the line  $x = z = 0$  normal to the interface or wall, we can expect the first derivatives of  $v, \rho, h, T$ , and  $Y_m$  with respect to either  $x$  or  $z$  to be zero-valued. For unsteady cases, only symmetric situations will be considered so that the stagnation point remains at the origin and the wall or interface remains at  $y = 0$ . The velocity components  $u$  and  $w$  will be odd functions of  $x$  and  $z$ , respectively, going through zero and changing the sign at that line. Consequently, upon neglect of terms of  $O(x^2)$  and  $O(z^2)$ , the variables  $v, \rho, h, T$ , and  $Y_m$  can be considered to be functions only of  $t$  and  $y$ . For steady flow, the density-weighted Illingworth transformation of  $y$  can be used to replace  $y$  with  $\eta \equiv \int_0^y \rho(y') dy'$ . Neglect of the same order of terms implies that  $u = S_1 x (df_1 / d\eta)$  and  $w = S_2 z (df_2 / d\eta)$ . Note that  $u$  is independent of  $z$  and  $w$  is independent of  $x$  in this case where no shear strain is imposed on the incoming stream(s). At the edge of the viscous layer at large positive  $\eta$ ,  $df_1 / d\eta \rightarrow 1$ ,  $df_2 / d\eta \rightarrow 1$ ,  $f_1 \rightarrow \eta$ , and  $f_2 \rightarrow \eta$ . We define  $(\prime) \equiv d(\prime) / d\eta$ . Note that other transformations of the  $y$  coordinate can be made, e.g., weighting by transport properties<sup>17,18</sup> rather than density.

Under the described situation, the following relations hold for the terms depending on viscous stress:

$$\begin{aligned} \frac{\partial \tau_{xj}}{\partial x_j} &= \rho^2 \mu x S_1 f_1'''' + \rho x S_1 f_1'' \frac{d(\rho \mu)}{d\eta}, \quad \frac{\partial \tau_{yj}}{\partial x_j} = \frac{4\rho}{3} \frac{d}{d\eta} \left( \rho \mu \frac{dv}{d\eta} \right) - \frac{2\rho}{3} (S_1 f_1' + S_2 f_2') \frac{d\mu}{d\eta} + \frac{\rho \mu}{3} (S_1 f_1'' + S_2 f_2''), \\ \frac{\partial \tau_{zj}}{\partial x_j} &= \rho^2 \mu z S_2 f_2'''' + \rho z S_2 f_2'' \frac{d(\rho \mu)}{d\eta}, \quad \frac{\partial (u_i \tau_{ij})}{\partial x_j} = \frac{4\rho}{3} \frac{d}{d\eta} \left( \rho \mu \frac{d(v^2/2)}{d\eta} \right) + \frac{4\mu}{3} \left[ (S_1 f_1')^2 + (S_2 f_2')^2 - S_1 S_2 f_1' f_2' - \rho (S_1 f_1' + S_2 f_2') \frac{dv}{d\eta} \right] \\ &+ \rho v \left[ \frac{\mu}{3} (S_1 f_1'' + S_2 f_2'') - \frac{2}{3} \frac{d\mu}{d\eta} (S_1 f_1' + S_2 f_2') \right]. \end{aligned} \tag{7}$$

In the nondimensional form given by Eqs. (1)–(7), the dimensional strain rates  $S_1^*$  and  $S_2^*$  are each normalized by the dimensional sum  $S_1^* + S_2^*$ . Thus, the nondimensional relation is  $S_2 = 1 - S_1$  and only one independent nondimensional strain-rate parameter is needed. Nevertheless, two strain rates are presented above and in the following analysis with the understanding that one depends on the other such that  $S_1 + S_2 = 1$ .  $S_1 + S_2$  will be explicitly stated in our analysis without substitution of the unity value. This choice clarifies whether a particular term when converted to a dimensional form depends on  $S_1^*$ ,  $S_2^*$  or the sum of the two strain rates.

For a steady state, the continuity equation (1) is readily integrated to give

$$\rho v = -S_1 f_1(\eta) - S_2 f_2(\eta) \tag{8}$$

and then

$$\frac{dv}{d\eta} = \frac{S_1 f_1(\eta) + S_2 f_2(\eta)}{\rho^2} \frac{d\rho}{d\eta} - \frac{S_1 f_1'(\eta) + S_2 f_2'(\eta)}{\rho} \tag{9}$$

Thus, the incoming inviscid flow outside the boundary layer is described by  $v = -(S_1 + S_2)\eta$  for positive  $\eta$  and  $v = -(S_1 + S_2)\eta/\rho_\infty$  for negative  $\eta$ . Note that the same result is found for the unsteady or steady incompressible state where there is no need to use  $\eta$  in place of  $y$  since  $\rho = 1$  everywhere. Then,  $v = -(S_1 + S_2)y$  for the external incoming flow.

Equations (7) and (8) may be substituted into Eq. (2) to determine the pressure gradient

$$\begin{aligned} \frac{\partial p}{\partial x} &= \rho[\rho\mu S_1 f_1''' + S_1 f_1''(\rho\mu)' + (S_1 f_1 + S_2 f_2)S_1 f_1'' - (S_1 f_1')^2]x, \\ \frac{\partial p}{\partial \eta} &= \frac{4}{3} \frac{d}{d\eta} (\rho\mu \frac{dv}{d\eta}) - \frac{2}{3} (S_1 f_1' + S_2 f_2') \frac{d\mu}{d\eta} + \frac{\mu}{3} (S_1 f_1'' + S_2 f_2'') \\ &\quad + (S_1 f_1 + S_2 f_2) \frac{\partial v}{\partial \eta}, \\ \frac{\partial p}{\partial z} &= \rho[\rho\mu S_2 f_2''' + S_2 f_2''(\rho\mu)' + (S_1 f_1 + S_2 f_2)S_2 f_2'' - (S_2 f_2')^2]z. \end{aligned} \tag{10}$$

It follows from the  $\eta$  pressure-gradient in Eq. (10) that  $\partial p/\partial \eta$  is a function only of  $\eta$ . Therefore,  $\partial^2 p/\partial x \partial \eta = 0$  and  $\partial^2 p/\partial z \partial \eta = 0$ . Now, the coefficient of  $x$  on the right side of the  $x$  pressure-gradient in Eq. (10) must be constant. The same conclusion is made for the coefficient of  $z$  on the right side of the  $z$  pressure-gradient in Eq. (10). At  $\eta = \infty$ ,  $f_1' = f_2' = 1$  and  $f_1'' = f_2'' = f_1''' = f_2''' = 0$  which allows the two constants to be determined. Specifically, we obtain

$$\begin{aligned} \rho\mu f_1''' + f_1''(\rho\mu)' + (S_1 f_1 + S_2 f_2) f_1'' + S_1 \left(\frac{1}{\rho} - (f_1')^2\right) &= 0, \\ \rho\mu f_2''' + f_2''(\rho\mu)' + (S_1 f_1 + S_2 f_2) f_2'' + S_2 \left(\frac{1}{\rho} - (f_2')^2\right) &= 0. \end{aligned} \tag{11}$$

In the outer flow with neglect of compressibility effects, the  $y$ -momentum equation becomes

$$\begin{aligned} \frac{\partial}{\partial \eta} \left[ p - \frac{4\rho\mu}{3} \frac{\partial v}{\partial \eta} \right] &= (S_1 f_1 + S_2 f_2) \frac{\partial v}{\partial \eta} = (S_1 + S_2) \eta \frac{\partial v}{\partial \eta} \\ &= - (S_1 + S_2)^2 \frac{\eta}{\rho_\infty}. \end{aligned} \tag{12}$$

For steady flows,  $S_1 + S_2 = 1$ . The dependence of  $v$  on  $f \equiv S_1 f_1 + S_2 f_2$  is shown by Eq. (8). Thus, the function  $f$  will be important in

determining both the field for  $v$  and the scalar fields. From Eq. (11), an equation for  $f$  can be formed

$$\rho\mu f'''' + f''(\rho\mu)' + ff'' + \frac{1}{\rho} - (f')^2 = 2S_1 S_2 \left(\frac{1}{\rho} - f_1' f_2'\right). \tag{13}$$

Consequently,  $f$  will depend on both  $S_1$  and  $S_2$ , not merely on  $S_1 + S_2$ . The particular distribution of the normal strain rate between the two transverse directions will matter. In our calculations, emphasis will be placed on the planar case ( $S_1 = 0, S_2 = 1.0$ ) where the product  $S_1 S_2$  is minimized, a fully three-dimensional case ( $S_1 = 0.25, S_2 = 0.75$ ), and the axisymmetric case ( $S_1 = S_2 = 0.5$ ) where the product  $S_1 S_2$  is maximized. The reasons for bounding the parameter ( $0 \leq S_1 \leq 0.5$ ) will be explained below.

The above equations can be readily applied for nonreacting counterflow, wall stagnation-point flow, and diffusion-flame counterflows as will be explained in Secs. III–V, respectively. First, we will treat the nonreacting counterflow in Sec. III.

### III. 3D COUNTERFLOW

For the counterflow, the boundary conditions for Eqs. (11) and (12) are

$$\begin{aligned} f_1'(\infty) &= \sqrt{\rho_\infty} f_1'(-\infty) = f_2'(\infty) = \sqrt{\rho_\infty} f_2'(-\infty) = 1, \\ f_1(0) &= f_2(0) = 0, \\ v(\infty) &= -(S_1 + S_2)\eta = -(S_1 + S_2)y, \\ v(-\infty) &= -(S_1 + S_2) \frac{\eta}{\rho_\infty^{3/2}} = -(S_1 + S_2) \frac{y}{\sqrt{\rho_\infty}}, \\ h(\infty) &= h_\infty, \quad h(-\infty) = h_{-\infty}, \\ Y_m(\infty) &= Y_{m,\infty}, \quad Y_m(-\infty) = Y_{m,-\infty}. \end{aligned} \tag{14}$$

Thus, at plus infinity,  $f_1$  and  $f_2$  both behave as  $\eta$ , while at minus infinity, they both behave as  $\eta/\sqrt{\rho_\infty}$ .

The values of  $v$  do not asymptote to a constant at  $+\infty$  or  $-\infty$ ; we therefore will take the boundary values for  $v$  at  $y^*$  positions whose magnitudes are severalfold the expected viscous-layer thickness,  $[\mu_\infty^*/(\rho_\infty^*(S_1^* + S_2^*))]^{1/2}$ . So,  $+\infty$  is approximated by a value of  $y \gg 1$  or  $\eta \gg 1$ , while  $-\infty$  is approximated by a value of  $|y| \gg 1$  or  $|\eta| \gg \rho_\infty$ . Variable density due to temperature variation will be addressed. However, compressibility effects within the viscous layer will be assumed to be negligible. The magnitude of the dimensional velocity at the layer edge is  $[(S_1^* + S_2^*)\mu_\infty^*/\rho_\infty^*]^{1/2}$ ; thus, the kinetic energy per mass based on that velocity magnitude will be assumed to be small compared to the ambient enthalpy values.

Equations (11), (12), and (14) will apply here in Subsections III A–III C and in Sec. IV. They will couple with the equations that describe the scalar fields.

#### A. Steady incompressible counterflow

For the steady incompressible flow with constant properties ( $\mu = 1, \rho = 1$ ) everywhere including the boundary values at plus and minus infinity, Eq. (11) and its boundary conditions may be recast as follows:



$$\begin{aligned}
 f_1''' + (S_1 f_1 + S_2 f_2) f_1'' + S_1 (1 - (f_1')^2) &= 0, \\
 f_2''' + (S_1 f_1 + S_2 f_2) f_2'' + S_2 (1 - (f_2')^2) &= 0, \\
 f_1(0) = f_2(0) = 0; \quad f_1'(\infty) = f_1'(-\infty) = f_2'(\infty) = f_2'(-\infty) &= 1. \quad (15)
 \end{aligned}$$

The solutions now for Eqs. (15) and (10) can be found by inspection, namely,

$$\begin{aligned}
 f_1(\eta) = f_2(\eta) = \eta, \quad f_1(\eta)' = f_2(\eta)' &= 1, \\
 f_1(\eta)'' = f_2(\eta)'' = 0, \quad f_1(\eta)''' = f_2(\eta)''' &= 0, \\
 u = -S_1 x, \quad v = -(S_1 + S_2)y, \quad w = S_2 z, \\
 p = p_{ref} - \frac{(S_1 x)^2}{2} - \frac{[(S_1 + S_2)y]^2}{2} - \frac{(S_2 z)^2}{2}. \quad (16)
 \end{aligned}$$

The reference pressure is the pressure at the stagnation point here. In this incompressible solution, there is no viscous shear and the normal strain and viscous normal stress are uniform; thus, there is no viscous force and a viscous interface layer does not appear. The solution is an exact solution of the Navier-Stokes equation with neglect of terms of  $O(x^2)$  and  $O(z^2)$ . No neglect of higher powers in  $y$  has been made; the boundary-layer approximation has not been invoked. The solution for pressure throughout the flow is identical to the inviscid-counterflow pressure solution. This will not occur for the variable-density case. Furthermore, it is noteworthy that the viscous dissipation rate is uniform and positive valued. That point will be discussed in Subsection III B.

For the incompressible case, we can simplify Eqs. (4) and (5) by neglecting kinetic energy and other terms of  $O(v^2)$  compared to thermal energy. Also, we do not consider chemical reaction and do assume  $Le$  and  $\lambda/c_p$  are constant. Thus,

$$\frac{\lambda}{c_p} \frac{d^2 h}{dy^2} + (S_1 + S_2)y \frac{dh}{dy} = 0, \quad (17)$$

$$\frac{\lambda}{c_p} \frac{d^2 Y_m}{dy^2} + Le(S_1 + S_2)y \frac{dY_m}{dy} = 0; \quad m = 1, 2, \dots, N. \quad (18)$$

For the steady state, we obtain linear ordinary homogeneous differential equations. The boundary conditions at plus infinity and minus infinity are set yielding the solutions

$$\begin{aligned}
 \frac{h - h_{-\infty}}{h_{\infty} - h_{-\infty}} &= \frac{1}{2} \left[ 1 + \operatorname{erf} \left( \sqrt{\frac{\rho c_p (S_1 + S_2)}{2\lambda}} y \right) \right], \\
 \frac{Y_m - Y_{m,-\infty}}{Y_{m,\infty} - Y_{m,-\infty}} &= \frac{1}{2} \left[ 1 + \operatorname{erf} \left( \sqrt{\frac{Le \rho c_p (S_1 + S_2)}{2\lambda}} y \right) \right], \\
 m &= 1, 2, \dots, N. \quad (19)
 \end{aligned}$$

### B. Unsteady incompressible counterflow

The unsteady, incompressible counterflow case is also readily solved. If strain rates and/or far-stream pressure are time dependent, the solution is given in terms of  $S_1(t)$ ,  $S_2(t)$  and/or  $p_{ref}(t)$

$$\begin{aligned}
 u &= -S_1(t)x, \quad v = -[S_1(t) + S_2(t)]y, \quad w = S_2(t)z, \\
 p &= p_{ref}(t) - \left[ \frac{dS_1}{dt} + S_1^2 \right] \frac{x^2}{2} - \left[ \frac{d(S_1 + S_2)}{dt} + (S_1 + S_2)^2 \right] \frac{y^2}{2} \\
 &\quad - \left[ \frac{dS_2}{dt} + S_2^2 \right] \frac{z^2}{2}. \quad (20)
 \end{aligned}$$

Note that in this unsteady case, the normalized  $S_1(t) + S_2(t)$  need not sum to unity;  $S_1(t)$  and  $S_2(t)$  should be considered as independent. The reference or initial value will be normalized to have unity value.

Solutions for the unsteady incompressible energy and species Eqs. (17) and (18) are also possible in the unsteady state with constant  $\lambda/(\rho c_p)$  and  $Le = 1$ .

For the unsteady incompressible case, we have

$$\frac{\partial h}{\partial t} - (S_1 + S_2)y \frac{\partial h}{\partial y} - \frac{\partial p}{\partial t} = \frac{\lambda}{c_p} \frac{\partial^2 h}{\partial y^2}, \quad (21)$$

$$\frac{\partial Y_m}{\partial t} - (S_1 + S_2)y \frac{\partial Y_m}{\partial y} = \frac{\lambda}{Le c_p} \frac{\partial^2 Y_m}{\partial y^2}, \quad m = 1, 2, \dots, N. \quad (22)$$

Equation (21) neglects viscous dissipation  $(\partial u_i / \partial x_j) \tau_{ij}$  and the spatial variation of pressure, both of which are of the order of the square of the Mach number.

The pressures in the incoming streams are assumed steady with the unsteadiness in the strain rates. Certain transformations are useful. They were also used by Marble,<sup>2</sup> Karagozian and Marble,<sup>3</sup> and Cetegen and Sirignano<sup>4,5</sup>

$$\tau \equiv \int_0^t e^{\int_0^{t'} 2(S_1 + S_2) dt''} dt'; \quad \xi \equiv y e^{\int_0^t (S_1 + S_2) dt'}. \quad (23)$$

Following a material element, the value of  $\xi$  remains constant. The transformed equations for heat and mass transfer become

$$\frac{\partial h}{\partial \tau} = \frac{\lambda}{\rho c_p} \frac{\partial^2 h}{\partial \xi^2}, \quad \frac{\partial Y_m}{\partial \tau} = \frac{\lambda}{Le \rho c_p} \frac{\partial^2 Y_m}{\partial \xi^2}, \quad m = 1, 2, \dots, N. \quad (24)$$

The well known solutions are

$$\begin{aligned}
 \frac{h - h_{-\infty}}{h_{\infty} - h_{-\infty}} &= \frac{1}{2} \left[ 1 + \operatorname{erf} \left( \sqrt{\frac{\rho c_p}{4\lambda \tau}} \xi \right) \right] = \frac{1}{2} \left[ 1 + \operatorname{erf} \left( \sqrt{\frac{\rho c_p}{4\lambda \int_0^t \exp[\int_0^{t'} 2(S_1 + S_2) dt''] dt'}} y \exp \left[ \int_0^t (S_1 + S_2) dt' \right] \right) \right], \\
 \frac{Y_m - Y_{m,-\infty}}{Y_{m,\infty} - Y_{m,-\infty}} &= \frac{1}{2} \left[ 1 + \operatorname{erf} \left( \sqrt{\frac{Le \rho c_p}{4\lambda \int_0^t \exp[\int_0^{t'} 2(S_1 + S_2) dt''] dt'}} y \exp \left[ \int_0^t (S_1 + S_2) dt' \right] \right) \right], \quad m = 1, 2, \dots, N. \quad (25)
 \end{aligned}$$

The incompressible steady or unsteady counterflow does experience diffusion of heat and/or mass from one flow toward the other when the two opposing, incoming streams have differing temperature and/or composition. Since the two incoming streams have the same  $x$ -momentum,  $y$ -momentum magnitude, and  $z$ -momentum, there is no diffusion of momentum from one stream toward the other. Here, although there is a nonzero  $dv/dy$  value through the viscous layer, it is not caused by diffusion but rather by the pressure gradient, i.e., it is independent of  $\mu$  and the same velocity solutions for  $u$ ,  $v$ , and  $w$  occur if  $\mu = 0$ . In the variable density case, the variation of density and/or properties through the interface layer does result in diffusion of momentum from one stream toward another.

The maximum heat or mass flux at any instant of time occurs at  $y = 0$ . With the definition

$$\kappa(t) \equiv \sqrt{\frac{\exp\left[2 \int_0^t (S_1 + S_2) dt'\right]}{\int_0^t \exp\left[\int_0^{t'} 2(S_1 + S_2) dt''\right] dt'}}, \quad (26)$$

the maximum instantaneous value of the heat flux is  $(\kappa/2)\sqrt{\rho c_p/\pi\lambda}$  and the maximum for flux of the mass fraction is  $(\kappa/2)\sqrt{Le\rho c_p/\pi\lambda}$ . The variation of  $\kappa$  with time is shown in Fig. 1 for three cases of variation of the nondimensional normal strain rate in the  $y$ -direction: exponential decay to an asymptote of  $S_1 + S_1 = 1$ , exponential growth to the same asymptote, and cosinusoidal oscillation about the same value.  $\kappa$  asymptotes to the value of  $\sqrt{2}$  in the first two cases, while it oscillates about that value in the third case. The average value in the oscillation is a little lower than  $\sqrt{2}$ , and the wave shape becomes steeper on the rise side than on the decline side.

In both the steady and unsteady incompressible counterflows, all three velocity components are linear in the spatial coordinate variables. Thereby, second derivatives of velocity are everywhere zero, yielding zero viscous force everywhere. However, the constant first derivatives result in a uniform viscous dissipation rate over the full space, amounting to a uniform heat source which is being neglected here. In particular,  $(\partial u_i/\partial x_j)\tau_{ij} = 4\mu(S_1^2 + S_1S_2 + S_2^2)$ . This same value of the viscous dissipation rate will occur asymptotically outside the viscous layer for the variable-density counterflow and the constant-density and variable density wall-stagnation flows. Thus, a heat-source term that would appear in Eqs. (17) and (21) is ignored here, assuming its effect is minor for our situations where kinetic energy is small compared to thermal energy. Although counterflows

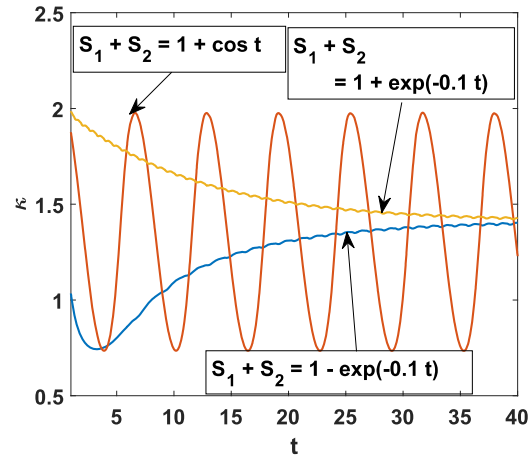


FIG. 1. Solutions for  $\kappa$  vs time in incompressible unsteady counterflow for three varying strain rates.

and wall-stagnation flows are posed theoretically as extending to infinity, the curvature of the counterflow interface or wall will limit the domain size. Thereby, this small heat source does not in practice extend over an infinite domain and its global impact remains small. This conclusion will apply to the variable-density flows as well.

For the incompressible counterflow case, the results here for the velocity fields can be extended to the case where two streams are incoming (say, in the  $y$  and  $x$  directions) and only one (say in the  $z$  direction) is outgoing; i.e.,  $S_1 < 0$  but  $S_1 + S_2 > 0$ . The reason is that  $u$  and  $w$  do not vary with  $y$ ; so, a plausible incoming stream from the  $x$ -direction occurs. (Of course, the flow in the  $z$  and  $y$  directions could be incoming with outgoing flow in the  $x$  direction.) However, inflow conditions on one stream for the scalar variables would have to be too contrived to make those scalar results useful in that case. That is, the scalar variables for incoming flow in the  $x$  (or  $z$ ) direction would have to satisfy specifically the  $y$  dependence given by Eq. (19) or (25).

### C. Variable-density counterflow

The variable density and viscosity case requires some couplings with Eqs. (4) and (5) and with an equation of state and fluid-property laws which affect  $\rho$  and  $\mu$ .

The pressure derivative can be determined by substituting from Eqs. (8) and (9) into (12)

$$\begin{aligned} \frac{\partial p}{\partial \eta} &= \frac{4}{3} \frac{d}{d\eta} \left( \rho \mu \left[ \frac{S_1 f_1(\eta) + S_2 f_2(\eta)}{\rho^2} \frac{d\rho}{d\eta} - \frac{S_1 f_1'(\eta) + S_2 f_2'(\eta)}{\rho} \right] \right) + \frac{\mu}{3} (S_1 f_1'' + S_2 f_2'') - \frac{2}{3} (S_1 f_1' + S_2 f_2') \frac{d\mu}{d\eta} \\ &\quad + (S_1 f_1 + S_2 f_2) \left[ \frac{S_1 f_1(\eta) + S_2 f_2(\eta)}{\rho^2} \frac{d\rho}{d\eta} - \frac{S_1 f_1'(\eta) + S_2 f_2'(\eta)}{\rho} \right], \\ p(x, \eta, z) &= p_{ref} + \frac{4\mu(\eta)}{3\rho(\eta)} \left[ (S_1 f_1(\eta) + S_2 f_2(\eta)) \frac{d\rho}{d\eta} - \rho(\eta) (S_1 f_1'(\eta) + S_2 f_2'(\eta)) \right] + \frac{4\mu(0)}{3} (S_1 f_1'(0) + S_2 f_2'(0)) + \int_0^\eta \left[ \frac{\mu(\zeta)}{3} (S_1 f_1''(\zeta) + S_2 f_2''(\zeta)) \right. \\ &\quad \left. - \frac{2}{3} (S_1 f_1'(\zeta) + S_2 f_2'(\zeta)) \frac{d\mu}{d\zeta} \right] d\zeta + \int_0^\eta (S_1 f_1(\zeta) + S_2 f_2(\zeta)) \left[ \frac{S_1 f_1(\zeta) + S_2 f_2(\zeta)}{\rho(\zeta)^2} \frac{d\rho}{d\zeta} - \frac{S_1 f_1'(\zeta) + S_2 f_2'(\zeta)}{\rho(\zeta)} \right] d\zeta - \frac{S_1^2 x^2}{2} - \frac{S_2^2 z^2}{2}. \quad (27) \end{aligned}$$

An exact solution of the variable-density Navier-Stokes equation has been obtained subject to determination of  $\rho$  and  $\mu$  through solutions of the energy and species equations as discussed below. There has been no need for use of a boundary-layer approximation. Thus, the solution here is the natural solution, subject to neglect of terms of  $O(x^2)$  and  $O(z^2)$ . Unlike the incompressible counterflow, a viscous layer exists with the three normal strains and normal viscous stresses varying through the layer due to varying density and viscosity. Shear strain also exists.

Consider the nonreacting, steady case; the terms with heats of formation in Eq. (6) are then properly neglected. With neglect of terms of  $O(x^2)$  and  $O(z^2)$ , the quantity  $\tilde{H} \equiv h + u_k u_k / 2 \approx h + v^2 / 2 = \tilde{H}(\eta)$ . Substitution from Eq. (7) yields

$$\begin{aligned} \rho v \frac{d\tilde{H}}{d\eta} &= \frac{d}{d\eta} \left( \frac{\rho\lambda}{c_p} \frac{dh}{d\eta} \right) + \frac{4}{3} \frac{d}{d\eta} \left( \rho\mu \frac{d(v^2/2)}{d\eta} \right) \\ &+ \frac{4\mu}{3\rho} \left[ (S_1 f_1')^2 + (S_2 f_2')^2 - S_1 S_2 f_1' f_2' \right] \\ &- \frac{4\mu}{3} (S_1 f_1' + S_2 f_2') \frac{dv}{d\eta} \\ &+ v \left[ \frac{\mu}{3} (S_1 f_1'' + S_2 f_2'') - \frac{2}{3} \frac{d\mu}{d\eta} (S_1 f_1' + S_2 f_2') \right]. \end{aligned} \quad (28)$$

$Le = 1$  is implied here. If consideration of the total energy  $\tilde{H}$  including kinetic energy is desired, it is convenient to assume a constant Prandtl number  $Pr \equiv \mu c_p / \lambda = 3/4$ . This is actually better than the more common  $Pr = 1$  assumption. White<sup>13</sup> on Page 42 shows that for seven common gases over a temperature range to 2000 °R,  $0.66 < Pr < 0.80$ . That value of  $Pr$  is commonly used in the analysis of flows where normal viscous stress is dominant, e.g., weak shock structure studies.<sup>25</sup>

Combine the first two terms on the right side of Eq. (28), and use Eq. (8) to substitute for  $v$  and  $dv/d\eta$ . Define

$$\begin{aligned} F(\eta) &\equiv \frac{4\mu}{3} (S_1 f_1' + S_2 f_2') \left[ \frac{S_1 f_1(\eta) + S_2 f_2(\eta)}{\rho^2} \frac{d\rho}{d\eta} - \frac{S_1 f_1'(\eta) + S_2 f_2'(\eta)}{\rho} \right] \\ &- \frac{4\mu}{3\rho} \left[ (S_1 f_1')^2 + (S_2 f_2')^2 - S_1 S_2 f_1' f_2' \right] \\ &+ \frac{\mu}{3\rho} (S_1 f_1'' + S_2 f_2'') (S_1 f_1 + S_2 f_2) \\ &- \frac{2}{3\rho} \frac{d\mu}{d\eta} (S_1 f_1' + S_2 f_2') (S_1 f_1 + S_2 f_2). \end{aligned} \quad (29)$$

Note that  $F(\eta) = O(v^2)$ . Substitute from Eq. (8) to have

$$\frac{4\rho\mu}{3} \frac{d^2\tilde{H}}{d\eta^2} + \left[ S_1 f_1 + S_2 f_2 - \frac{4}{3} \frac{d(\rho\mu)}{d\eta} \right] \frac{d\tilde{H}}{d\eta} = F(\eta). \quad (30)$$

In the above analysis, no boundary-layer approximation was used. It remains to use thermodynamic relations to substitute for  $\rho$  and  $\mu$  in terms of  $h = \tilde{H} - v^2/2$  and  $p$ .

Now, we will address cases of low Mach numbers where  $\tilde{H} \approx h$  gives an acceptable result. Let us examine the special case where

$\rho\mu = 1$ . Then, Eqs. (11) and (14) yield

$$\begin{aligned} f_1'''' + (S_1 f_1 + S_2 f_2) f_1'' + S_1 [\tilde{h} - (f_1')^2] &= 0, \\ f_2'''' + (S_1 f_1 + S_2 f_2) f_2'' + S_2 [\tilde{h} - (f_2')^2] &= 0, \\ \tilde{h}'' + Pr(S_1 f_1 + S_2 f_2) \tilde{h}' &= 0, \\ f_1'(\infty) = f_2'(\infty) = 1, \quad f_1'(-\infty) = f_2'(-\infty) &= \frac{1}{\sqrt{\rho-\infty}}, \\ f_1(0) = f_2(0) = 0, \quad \tilde{h}(\infty) = 1, \quad \tilde{h}(-\infty) &= \frac{1}{\rho-\infty}. \end{aligned} \quad (31)$$

In the above relation,  $\tilde{h}(\eta) \equiv h^*(\eta)/h^*(\infty) = h(\eta)/h_\infty$  and the required constants are  $S_1, S_2 = 1 - S_1, \rho-\infty$ , and  $Pr$ .

Equation (11) indicates a dependence of the heat and mass transport on  $f \equiv S_1 f_1 + S_2 f_2$ . Manipulation of the first two equations of (11) leads to an ODE for  $f$  with  $S_1 S_2$  and  $S_1 S_2 f_1' f_2'$  as parameters, clearly indicating that generally  $f$  will have a dependence on  $S_1 S_2$ . Thus, the behavior for the counterflow can vary from the planar value of  $S_1 = 1, S_2 = 0$  (or vice versa) or from the axisymmetric case  $S_1 = S_2 = 1/2$ . This clearly shows that distinctions must be made amongst the various possibilities for three-dimensional strain fields as  $S_1 S_2$  varies between large negative numbers and  $1/4$ . An exception will be the incompressible case with constant properties where the  $S_1 S_2$  terms cancel in the equation for  $f$ .

All of the terms in Eq. (29) are of  $O(v^2)$ . If we neglect that order,  $F \approx 0$  and  $\tilde{H} \approx h$ . Now, an assumption about  $Pr$  offers no advantage. Thereby, with  $\rho\mu = 1$ , we obtain

$$\frac{d^2 h}{d\eta^2} + Pr [S_1 f_1 + S_2 f_2] \frac{dh}{d\eta} \approx 0. \quad (32)$$

The effects of the normalized strain rates ( $S_1$  and  $S_2 = 1 - S_1$ ) are shown in Figs. 2 and 3. A simple inspection of the governing ODEs leads to the conclusion that the values for  $f_1, f_1', f_2, f_2', u/x$ , and  $w/z$  can be interchanged with the values for  $f_2, f_2', f_1, f_1', w/z$ , and  $u/x$ , when  $S_1$  and  $S_2$  are replaced by  $1 - S_1$  and  $1 - S_2$ , respectively. Thus, only values for  $S_1 \leq 0.5, S_2 \geq 0.5$  are reported.  $S_1 = 0, S_2 = 1.0$  is the planar (two-dimensional) case, while  $S_1 = 0.5 = S_2$  is the axisymmetric case. Note that for  $S_1 > 1$  or  $S_2 > 1$  (which imply  $S_2 < 0$  or  $S_1 < 0$ , respectively), there would be incoming streams from two directions. One incoming stream would have a prescribed velocity profile in the viscous layer determined as a local exact solution to the Navier-Stokes conditional on matching the profile determined by upstream conditions for the flow in that direction; this situation is too highly contrived and is not considered here. Thus,  $S_1$  and  $S_2$  are always each non-negative and bounded above by the unity value in our considerations here. The figures show results for three strain rates:  $S_1 = 0$  (planar case),  $S_1 = 0.25$  (3D strain), and  $S_1 = 0.5$  (axisymmetric case).

The results for the three-dimensional case, exemplified here by  $S_1 = 0.25$ , lie between the results for the planar case ( $S_1 = 0$ ) and the axisymmetric case ( $S_1 = 0.5$ ). The strain rate has no noticeable effect on  $f_2'$  which applies to the direction with the greater positive normal strain rate and a slight effect on  $f_1'$  for the lower strained direction. Consistently, there is little effect of strain rate on  $f_1$  and  $f_2$ . The term  $S_{1,2} [\tilde{h} - (f_{1,2}')^2]$  in Eq. (31) is too small to create a substantial effect; it is found to be typically two orders of magnitude smaller than the



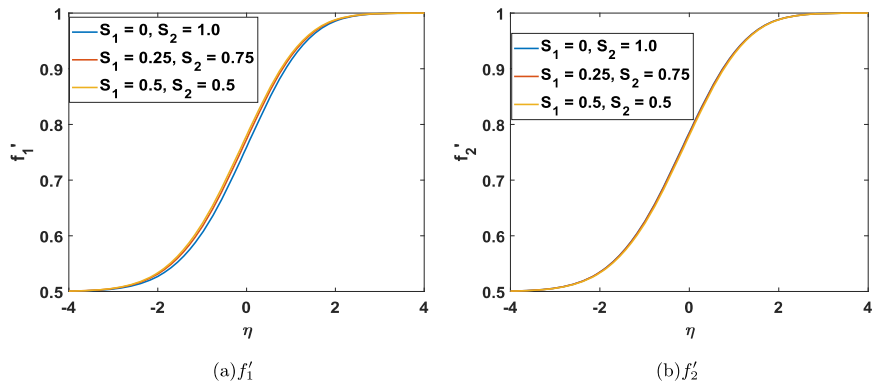


FIG. 2. Solutions for similarity variables. Counterflow with various strain rate distributions.  $Pr = 1.0$ ;  $h_{-\infty}/h_{\infty} = 0.25$ .

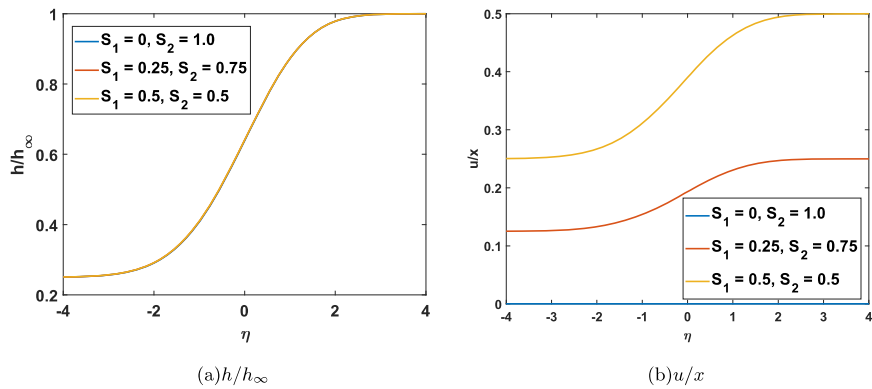
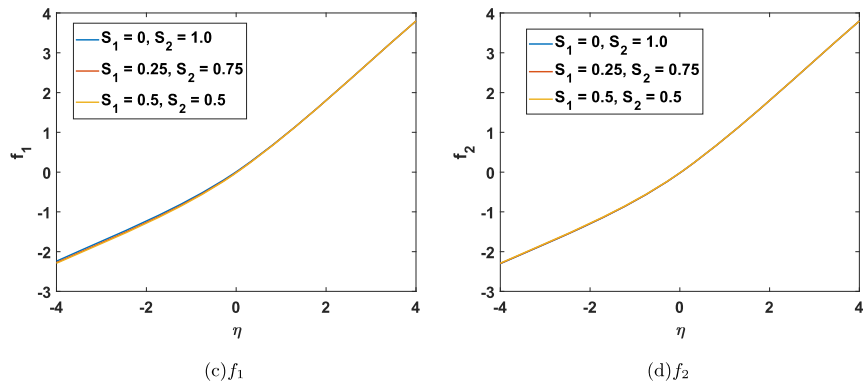
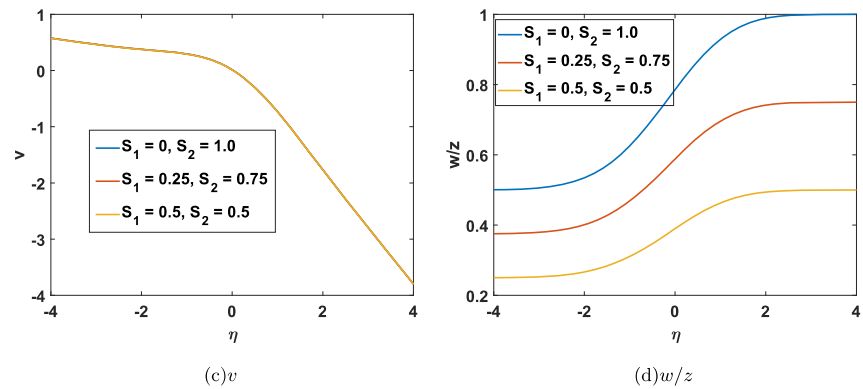
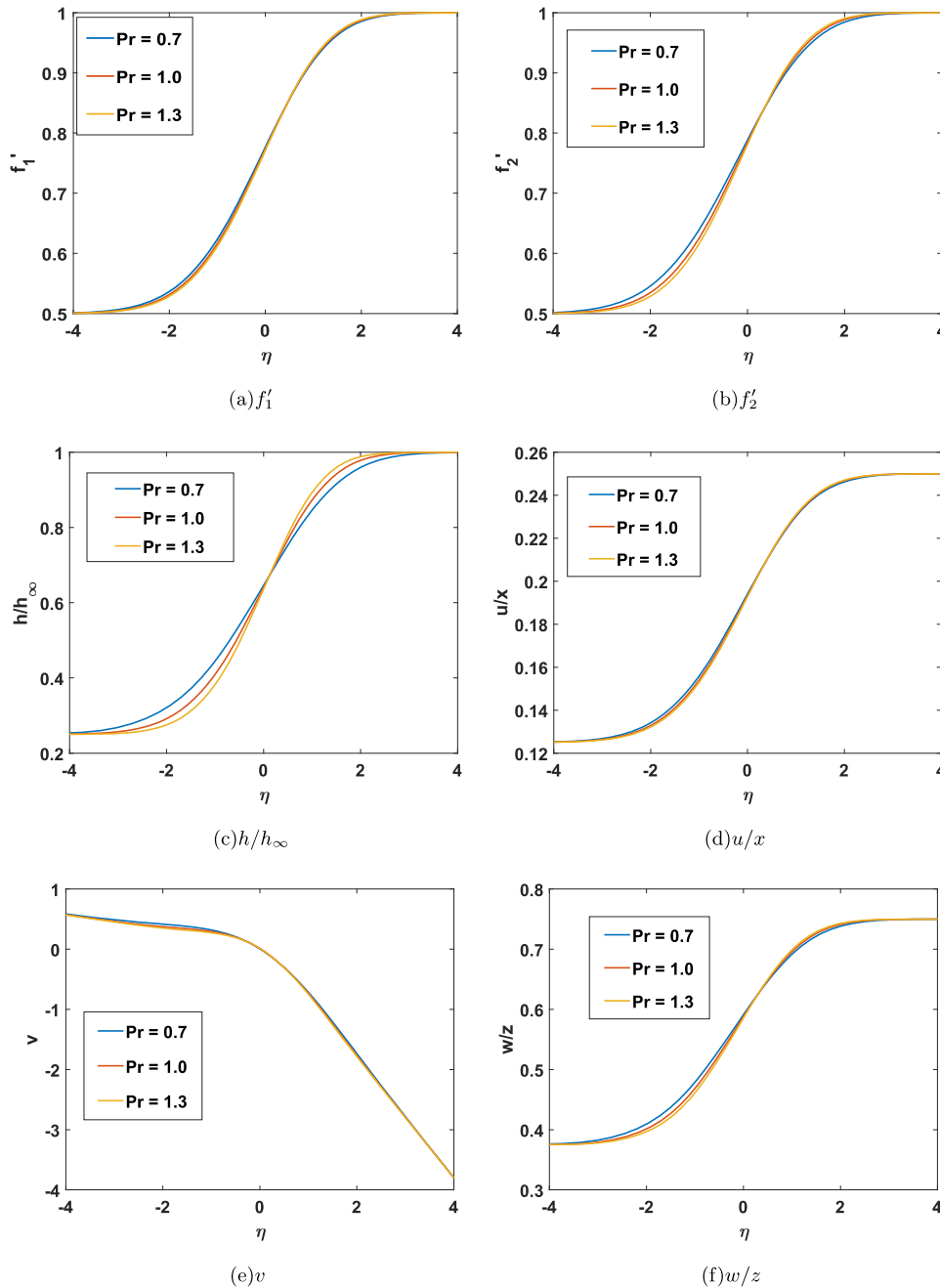


FIG. 3. Solutions for nondimensional velocities and enthalpy. Counterflow with various strain rate distributions.  $Pr = 1.0$ ;  $h_{-\infty}/h_{\infty} = 0.25$ .



$f_{1,2}f''_{1,2}$  term. The nondimensional enthalpy and the nondimensional velocity component  $v$  in the counterflow direction show no significant effect from the distribution of the transverse normal strain rate. The dimensional velocity component in the counterflow direction would scale with the square root of the dimensional strain rate. The values of  $u/x$  and  $w/z$  do depend strongly on the nondimensional strain rate in their respective directions with a direct proportion. The dimensional values  $u^*/x^*$  and  $w^*/z^*$  would then scale with the

dimensional strain rate in the  $y$ -direction. The influence of  $Pr$  is shown in Fig. 4. As expected, an increase in the value of  $Pr$  causes a larger gradient for the enthalpy variation. Interestingly, a similar steepening is caused for  $f'_1, f'_2, u/x,$  and  $w/z$ . Little effect is seen for the  $v$  component of velocity. The variation of  $1/\rho_{-\infty} = h/h_{\infty}$  is described in Fig. 5. Since the boundary conditions for  $h, f_1,$  and  $f_2$  at  $\eta = -\infty$  are substantially affected, there are strong consequences for the solutions, especially for negative  $\eta$ . The consequences are focused there



**FIG. 4.** Solutions for counterflow with various Prandtl numbers.  $S_1 = 0.25$ ;  $S_2 = 0.75$ ;  $h_{-\infty}/h_{\infty} = 0.25$ .

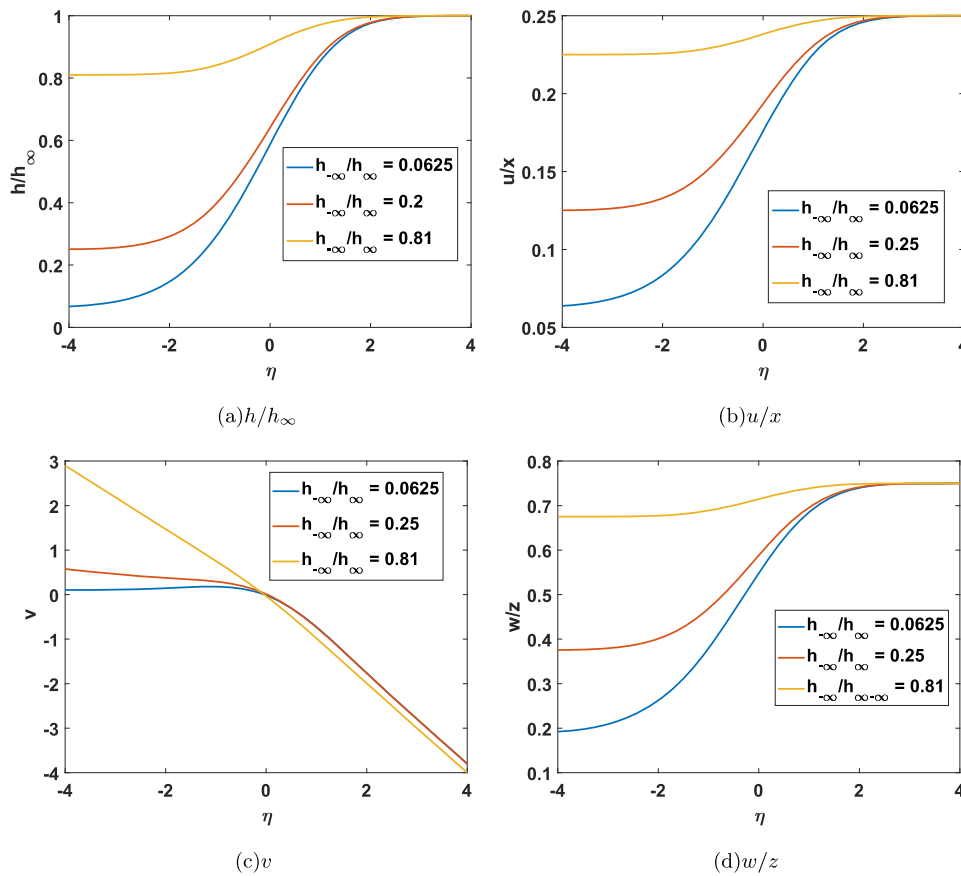


FIG. 5. Solutions for nondimensional velocities and enthalpy. Counterflow with various enthalpy ratios.  $S_1 = 0.25$ ;  $S_2 = 0.75$ ;  $Pr = 1.0$ .

since  $f_1(0) = f_2(0) = 0$  and  $f_1'(\infty) = f_2'(\infty) = 1$  are maintained for all the cases here. Note that the density weighting for the variable  $\eta$  makes the inflection stronger as the solution varies from the higher-density, negative- $\eta$  range to the lower-density, positive- $\eta$  range. See, for example, the curves for  $v$  vs  $\eta$ . As shown in Fig. 2,  $\rho v = S_1 f_1 + S_2 f_2$  is not generally linear in  $\eta$ . Hence, the solution for scalars obtained from diffusive-advective equations such as Eq. (32) will not yield error functions as commonly found with a constant-density assumption.<sup>6</sup> Equation (19) gives such an example of the constant-density assumption.

In related fashion to the incompressible counterflow, the variable-density results here for the velocity fields can in principle be extended to the case where two streams are incoming (say, in the  $y$  and  $x$  directions) and only one (say, in the  $z$  direction) is outgoing; i.e.,  $S_1 < 0$  but  $S_1 + S_2 > 0$ . However, now  $u$  and  $w$  do vary with  $y$ ; so, the inflow velocity conditions as well as the scalar variable conditions are not plausible.

#### IV. DIFFUSION FLAME WITH 3D STRAIN

For the diffusion flame in the counterflow configuration, Eqs. (8), (10), (11), (14), (27), and (28) still apply. With  $Le = 1$  and  $Pr = 3/4$  in the steady state,  $H$  from Eq. (6) is governed by the same operator appearing in Eq. (33). Consequently,

$$\frac{4\rho\mu}{3} \frac{d^2 H}{d\eta^2} + \left[ S_1 f_1 + S_2 f_2 - \frac{4}{3} \frac{d(\rho\mu)}{d\eta} \right] \frac{dH}{d\eta} = F(\eta). \quad (33)$$

In the above energy equation, we have retained the  $y$ -component of kinetic energy per unit mass in  $H$ . However, an order of magnitude analysis indicates that it can be neglected in practical situations. Specifically, for a practical fluid at moderate temperature, a value of  $v^{*2}$  of  $O(10^3 \text{ m/s})$  or greater is required for the kinetic energy to be at least one percent of the sensible enthalpy. Then, the viscous-layer thickness  $\delta^* = O(10^{3/2}/(S_1^* + S_2^*))$  and also  $\delta^{*2} = O(\mu^*/[\rho^*(S_1^* + S_2^*)])$  from the advective-diffusive balance of the governing equations. With practical values of  $\mu^*$  and  $\rho^*$ , the strain rate  $S_1^* + S_2^*$  will reach  $O(10^7/\text{s})$  or greater. This is much too large to allow chemical reaction and to hold a flame. So, here in this subsection, we redefine  $H \equiv h + \sum_{m=1}^N Y_m h_{f,m}$  neglecting the kinetic energy. Then, no assumption about  $Pr$  is made.

In general, each of the species equations must be solved. However, for the special case of a one-step chemical reaction, each species is consumed or produced at a rate in direct proportion to the rate of some other species that is produced or consumed. Therefore, the steady-state version of Eq. (5) with  $Le = 1$  can be written as

$$\rho v \frac{dY_m}{d\eta} - \frac{d}{d\eta} \left( \frac{\rho\mu}{Pr} \frac{dY_m}{d\eta} \right) = \dot{\omega}_m = \nu_m \omega_1, \quad m = 1, 2, \dots, N, \quad (34)$$

where  $\nu_m$  is a stoichiometric constant. Then, conserved scalars  $\alpha_m \equiv Y_m - Y_1$  will satisfy

$$\rho v \frac{d\alpha_m}{d\eta} - \frac{d}{d\eta} \left( \frac{\rho\mu}{Pr} \frac{d\alpha_m}{d\eta} \right) = 0, \quad m = 2, \dots, N. \quad (35)$$

For the case of a simple diffusion flame with  $Y_F$  and  $Y_O$  representing the mass fractions of fuel and oxidizer, the conserved scalar is  $\alpha = Y_F - \nu Y_O$ . The far incoming stream on one side (positive  $y$  and  $\eta$ ) has  $Y_F = 1$ , while the other far incoming stream (negative  $y$  and  $\eta$ ) has  $Y_O = 1$ . For a rapid reaction rate, a thin flame occurs and can be assumed to have zero thickness. The thin flame is positioned at the  $\eta$  value where  $\alpha = 0$ . At the  $\eta$  (or  $y$ ) position where  $\alpha = 0$ , the magnitude of the local value of  $\rho v \alpha - (\rho\mu/Pr)d\alpha/d\eta$  gives the burning rate (mass flux per area). It is the sum of transport into the thin flame of fuel vapor by advection and diffusion.

In Eq. (34), realize that the nondimensional reaction rate  $\omega_i$  becomes very small when the dimensional strain rate is much greater than the dimensional reaction rate. This can cause extinction of a flame due to the stretching effect. Extinction will not be examined here.

Let us examine the special case where  $\rho\mu = 1$  and  $Le = 1$ . We define the Shvab Zel'dovich variables  $\alpha \equiv Y_F - \nu Y_O$  and  $\beta \equiv \tilde{h} + \nu Y_O \tilde{Q}$ , where  $\tilde{Q}$  is the fuel heating value normalized by  $h^*(\infty)$ . Assuming that a thin flame results where  $Y_F = 0$ ,  $Y_O = 0$ , one can write  $\tilde{h} = \beta + \text{minimum}(0, \tilde{Q}\alpha)$ . Then, Eqs. (11) and (14) yield

$$\begin{aligned} f_1''' + (S_1 f_1 + S_2 f_2) f_1'' + S_1 [\tilde{h} - (f_1')^2] &= 0, \\ f_2''' + (S_1 f_1 + S_2 f_2) f_2'' + S_2 [\tilde{h} - (f_2')^2] &= 0, \\ \alpha'' + Pr(S_1 f_1 + S_2 f_2) \alpha' = 0, \quad \beta'' + Pr(S_1 f_1 + S_2 f_2) \beta' &= 0, \\ f_1'(\infty) = f_2'(\infty) = 1, \quad f_1'(-\infty) = f_2'(-\infty) &= \frac{1}{\sqrt{\rho-\infty}}, \\ f_1(0) = f_2(0) = 0, \\ \alpha(\infty) = 1, \quad \alpha(-\infty) = -\nu, \\ \beta(\infty) = 1, \quad \beta(-\infty) = \frac{1}{\rho-\infty} + \nu \tilde{Q} &= \frac{h-\infty}{h_\infty} + \nu \tilde{Q} \end{aligned} \quad (36)$$

In the above relations, the required constants are  $S_1, S_2 = 1 - S_1, \rho-\infty, \nu, \tilde{Q}, Pr$ .

Figures 6–8 give the computational results for  $Q = 10$ ,  $\nu = 0.25$ , and various values of  $S_1, S_2, Pr$ , and  $\rho-\infty$ . The solutions for the conserved scalars  $\alpha$  and  $\beta$  and the velocity component  $v$  are monotonic. However, the enthalpy  $\tilde{h}$  peaks at the reaction zone and all of the velocity components  $u, v$ , and  $w$  have overshoots in the low-density region around the reaction zone. Since the Burke-Schumann limit of the infinite reaction rate is employed, the reaction zone has zero thickness resulting in a cusped shape with a discontinuity of the first derivative for  $\tilde{h}$ . The rate of strain has modest affect on the scalar fields and  $v$ . Significant influence is seen on the  $u$  and  $w$  velocity components which each increases with normal strain values for their respective direction. Unlike the nonreacting counterflow, the term  $S_{1,2}[\tilde{h} - (f_{1,2}')^2]$  in Eq. (31) is large for the reacting flow; it is found to be of the same order of magnitude as the  $f_{1,2} f_{1,2}'$  term. Again, the results are readily extended since the values for  $u/x$  and  $w/z$  can be interchanged with the values for  $w/z$  and  $u/x$  when  $S_1$  and  $S_2$  are replaced by  $1 - S_1$  and  $1 - S_2$ , respectively.

The results for the scalar properties have increasing gradients as  $Pr$  increases. In Fig. 7, the domain of high temperature and low density is narrowed in  $\eta$  space as  $Pr$  increases because scalar gradients increase. Thereby, densities in the low-density region increase causing the domain width in  $y$  space to narrow even more as  $Pr$  increases. As a consequence of the increase in density, the magnitude of the velocity overshoot is decreased as  $Pr$  increases. Figure 8 shows that an increase in ambient temperature leads, as expected, to higher peak values of temperature and enthalpy and to a greater velocity overshoot for all components.

The mixture fraction is commonly defined as  $Z = (\alpha - \alpha_{-\infty}) / (\alpha_\infty - \alpha_{-\infty})$ . For pure fuel at  $+\infty$  and pure oxidizer at  $-\infty$ , we have  $Z = (Y_F - \nu Y_O + \nu Y_{O,-\infty}) / (Y_{F,\infty} + \nu Y_{O,-\infty})$ . Then,  $Z$  is a conserved scalar that varies monotonically from 0 at minus infinity to 1 at plus infinity. It is governed by the homogeneous forms of Eq. (5) for the unsteady state and Eq. (35) in the steady state. It has the steady solution  $Z = J(\eta) / J(\infty)$  where

$$\begin{aligned} I(\eta) &\equiv \int_{-\infty}^{\eta} \frac{3}{4\rho\mu} [S_1 f_1(\zeta) + S_2 f_2(\zeta)] d\zeta, \\ J(\eta) &\equiv \int_{-\infty}^{\eta} e^{-I(\eta')} d\eta'. \end{aligned} \quad (37)$$

If  $f \equiv S_1 f_1 + S_2 f_2$  were linear in  $\eta$ ,  $J(\eta)$  becomes an error function. However, whenever density varies across the counterflow, a linear behavior cannot occur.

Bilger<sup>26</sup> has emphasized the use of element-based mass fractions which become conserved scalars because chemistry does not destroy atoms but only changes molecules. This allows us to consider general chemical kinetics without the use of the one-step assumption. Define the element mass fraction for the atom identified by integer  $k$  as  $Y_k \equiv \sum_{m=1}^N a_{m,k} Y_m W_k / W_m$ , where  $a_{m,k}$ ,  $W_k$ , and  $W_m$  are the integer number of  $k$  atoms in molecule  $m$ , the atomic weight of  $k$ , and the molecular weight of  $m$ , respectively. Then,  $Y_k$  is a conserved scalar satisfying the homogeneous forms of the differential equations given by Eqs. (5) and (35) for the unsteady and steady states, respectively. Defining  $Z \equiv (Y_k - Y_{k,-\infty}) / (Y_{k,\infty} - Y_{k,-\infty})$ , it satisfies these equations with  $Z$  varying from 0 to 1. For any  $k$ , the steady-state solution is again  $Z = J(\eta) / J(\infty)$ .

In standard fashion,<sup>6</sup> the independent variables  $t$  and  $y$  can be replaced by  $\tau \equiv t$  and  $Z(y, t)$  in Eq. (5), respectively. The result is

$$\begin{aligned} \frac{\partial Y_m}{\partial \tau} &= 2\chi \frac{\partial^2 Y_m}{\partial Z^2} + \dot{\omega}_m = 0, \quad m = 1, 2, \dots, N, \\ \chi &\equiv \frac{D}{2} \left( \frac{\partial Z}{\partial y} \right)^2 = \frac{\rho^2 D}{2} \left( \frac{\partial Z}{\partial \eta} \right)^2 = \frac{\rho\mu}{2} \frac{e^{-2I(\eta)}}{J^2(\infty)}, \end{aligned} \quad (38)$$

where  $\chi$  is commonly named the scalar dissipation rate. However, for laminar flows, it is better described as a measure of the strain rate. In Eq. (38),  $\eta(Z) = J^{inv}(ZJ(\infty))$  must be substituted where  $J^{inv}$  is the inverse function of  $J$  which must be determined numerically or approximated. In a special case<sup>6</sup> where  $f_1$  and  $f_2$  are linear in  $\eta$  obtained through a constant-density assumption,  $J$  becomes an error function because the velocity component  $v$  becomes linear in  $\eta$  (and in  $y$ ). Results for  $v$  in Figs. 6(e), 7(e), and 8(e) show substantial nonlinearity in  $v$ ; in fact, a nonmonotonic character exists.  $\rho v$  is also nonlinear in  $\eta$ . The error function commonly appears in the counterflow-flame literature; it results because  $dv/dy$  becomes a negative constant based on the constant-density assumption. The cited

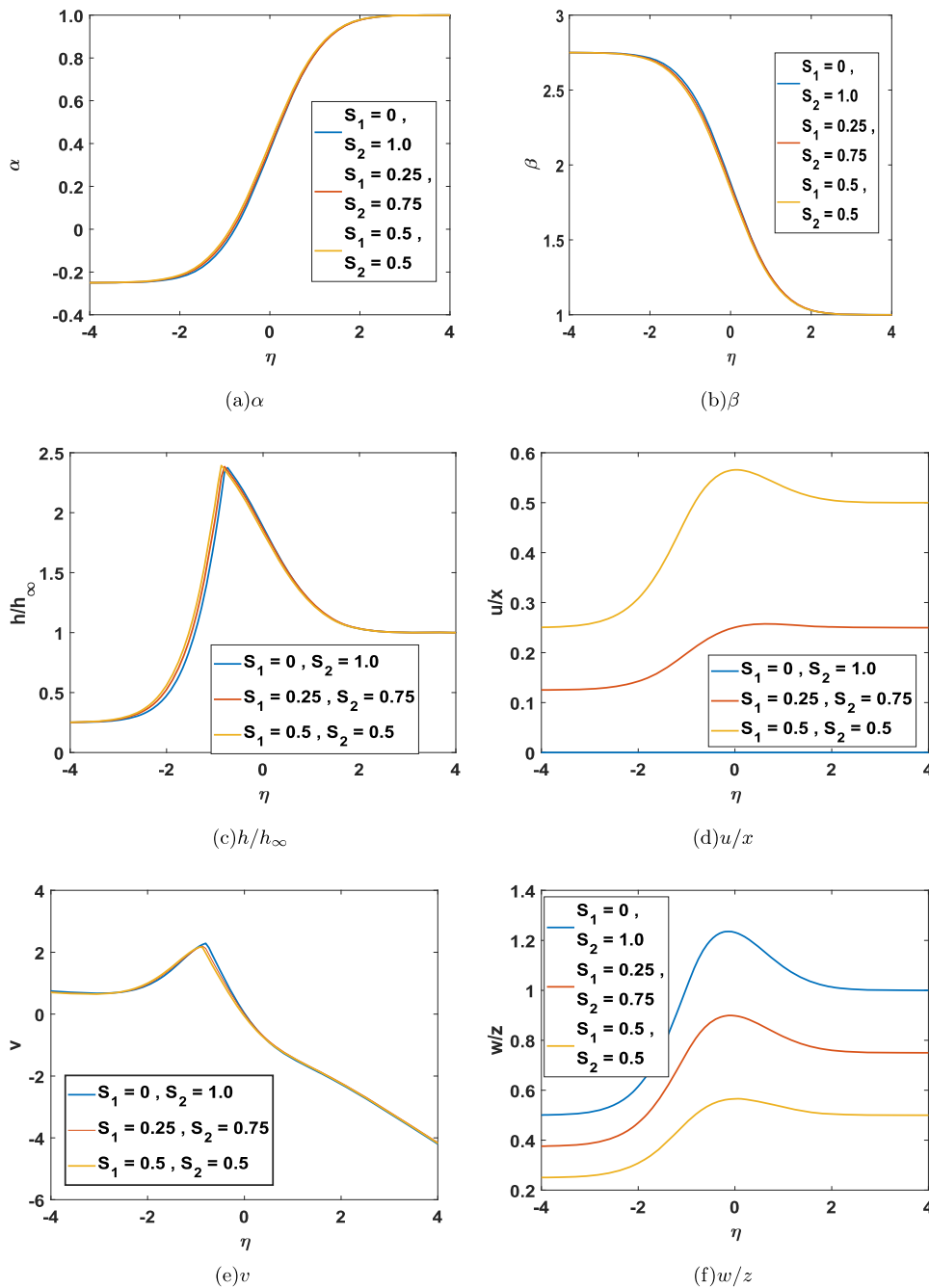


**FIG. 6.** Solutions for nondimensional velocities, conserved scalars, and enthalpy. Reacting counterflow with various strain rate distributions.  $Pr = 1.0$ ;  $h_\infty/h_\infty = 0.25$ .

subfigures not only show nonlinearity but, in addition, a change of sign for  $dv/d\eta$  (and consequently for  $dv/dy$ ). The constant-density assumption and the error-function results should not be used if accuracy is paramount.

In the steady state, the reaction rate in Eq. (38) is determined from the mass fractions using the known linear relations among temperature (from enthalpy for constant  $c_p$ ), mass fractions, and the conserved scalars  $Z$ ,  $\alpha$ , and  $\beta$ . So, a solution can be found in  $Z$ -space.

For the steady state with fast chemical kinetics,  $\dot{\omega}_m(Z)$  will have a significant value within a narrow region in  $Z$ -space around the stoichiometric value. On both sides of that narrow region,  $Y_m$  will be linear in  $Z$ .

Streamline shapes are especially interesting here because of both the unequal strain rates in the  $x$  and  $z$  directions and the flow expansion caused by heating from the combustion process. Given an initial point  $x_0, y_0,$  and  $z_0$  for a particle, the particle path (i.e., the



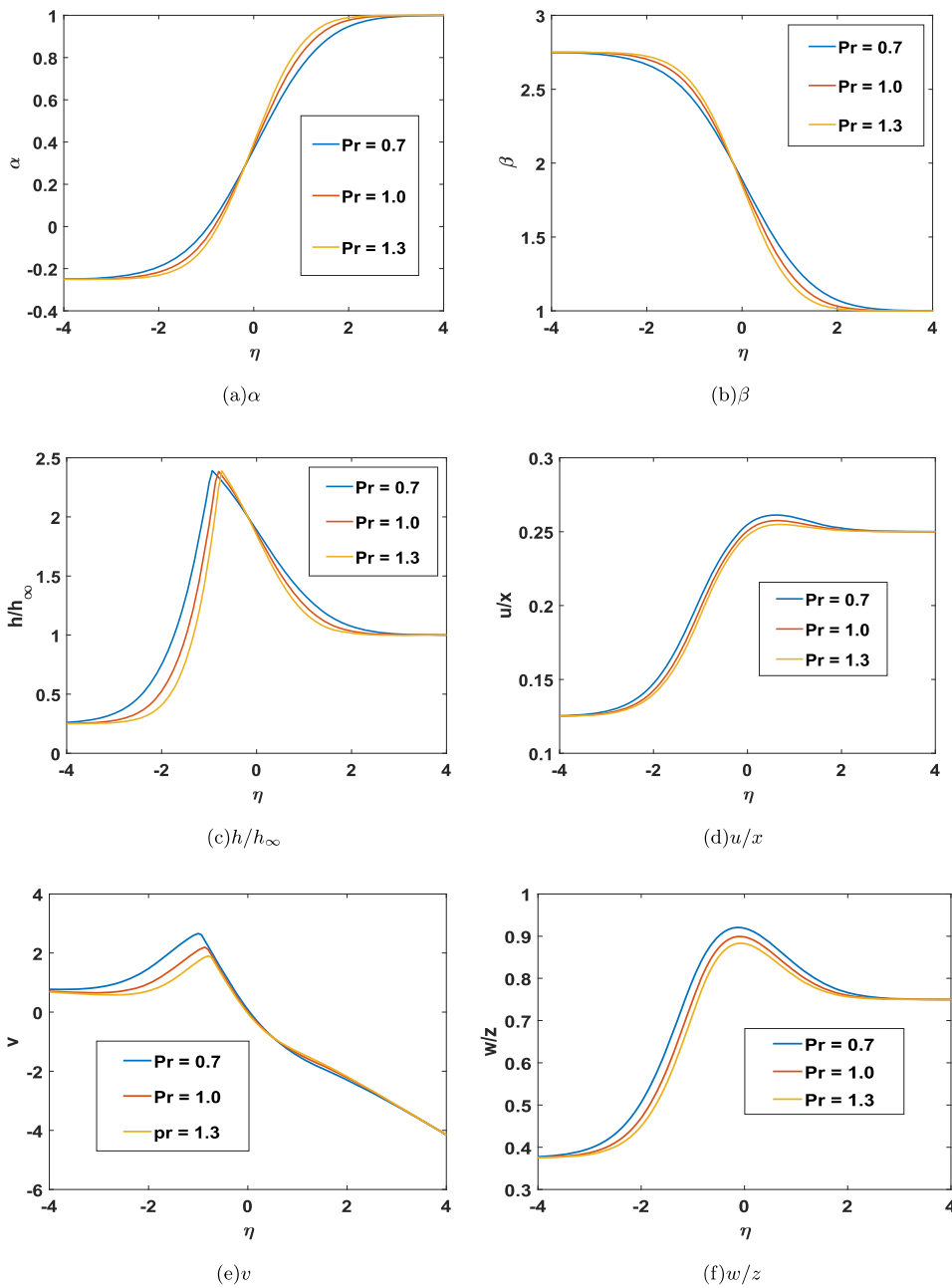


**FIG. 7.** Solutions for nondimensional velocities, conserved scalars, and enthalpy. Reacting counterflow with various Prandtl numbers.  $S_1 = 0.25$ ,  $S_2 = 0.75$ ;  $h_{-\infty}/h_\infty = 0.25$ .

streamline in a steady flow) can be obtained through integration of the following ordinary differential equations:

$$\frac{dx}{d\eta} = \frac{u}{\rho v} = -\frac{S_1 f_1' x}{S_1 f_1 + S_2 f_2}, \quad \frac{dy}{d\eta} = \frac{1}{\rho} = \tilde{h}, \quad \frac{dz}{d\eta} = -\frac{S_2 f_2' z}{S_1 f_1 + S_2 f_2}. \quad (39)$$

Clearly, the numerical solution following separation of variables is straightforward. Let us examine the case of Figs. 6 and 8 where  $S_1 = 0.25$ ,  $S_2 = 0.75$ ,  $Pr = 1.0$ , and  $h_{-\infty} = h_\infty$ . Realize as shown by Fig. 8(c) that heat release and enthalpy are maximum in the

region of negative  $\eta$  within the upward flow region. Therefore, a density minimum and local maxima of the velocity components occur there.

Figure 9(a) shows that the burning region with the local density minimum experiences larger changes in  $y$  for a given change in  $\eta$ . Subsequently, we see in the streamline projections of Figs. 9(b) and 9(c) that streamlines in the negative- $y$  upward flow region are stretched vertically more than in the downward flow. The streamline projections are the same for any  $x, y$  plane; that is, they do not depend on the  $z$  value. Likewise, the streamline projection

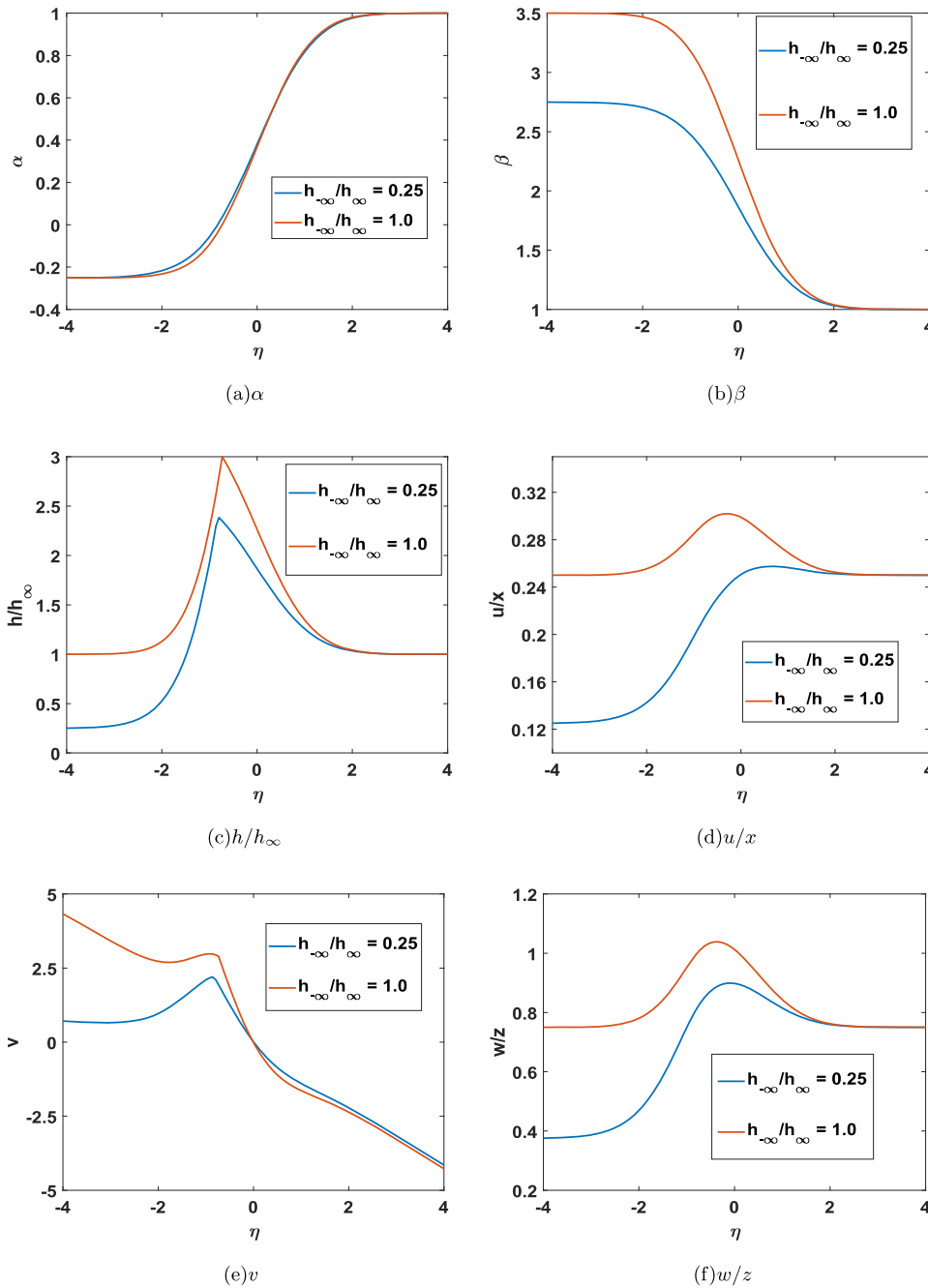


**FIG. 8.** Solutions for nondimensional velocities, conserved scalars, and enthalpy. Reacting counterflow with various enthalpy ratios.  $S_1 = 0.25$ ,  $S_2 = 0.75$ ;  $Pr = 1.0$ .

onto any the  $y, z$  plane is identical and without  $x$  dependence. However, the streamline projection onto an  $x, z$  plane will vary depending on the value of  $y$  (or equivalently  $\eta$ ). The effects of different ambient temperatures and density for the two opposing streams, obviously, will have an impact on the variations of streamline projections onto the  $x-z$  plane for both reacting and nonreacting counterflows. Also, it will affect wall-stagnation flows where wall temperature and ambient temperature differ, causing density gradients.

From Eq. (39), we can write

$$\frac{dz}{dx} = \frac{w}{u} = \Lambda(\eta) \frac{z}{u}, \quad \Lambda \equiv \frac{S_2 f_2'}{S_1 f_1'} \quad (40)$$

This will yield a power-law streamline projection  $z/z_0 = (x/x_0)^{\Lambda(\eta)}$ . The projections in the  $x, z$  plane will have symmetries at about both the  $x$  axis and the  $z$  axis.  $x$  and  $y$  will maintain the same sign along the streamline as  $x_0$  and  $z_0$ , respectively; i.e., the streamline will

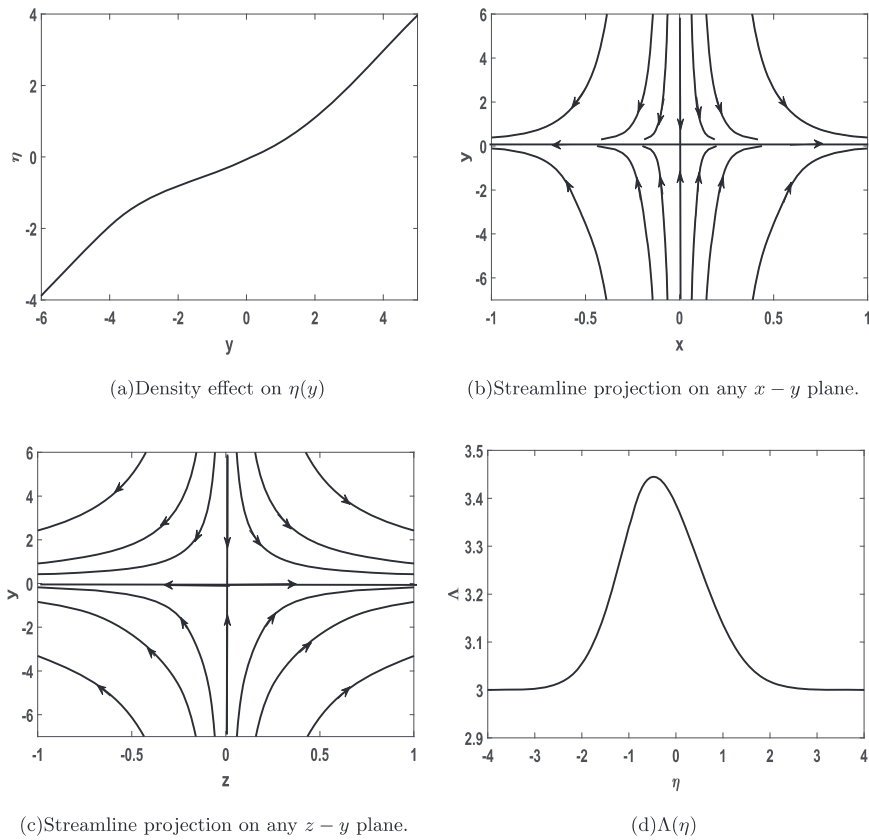


**FIG. 9.** Selected streamline projections.  $S_1 = 0.25$ ,  $S_2 = 0.75$ ;  $Pr = 1.0$ ;  $h_{-\infty}/h_{\infty} = 1.0$ .

not cross a symmetry plane at  $x = 0$  or  $z = 0$ . As shown in Fig. 9(d),  $\Lambda > 1$  in this case with a peak in the hot, low-density zone.  $z/x = \tan \theta$  where  $\theta$  is the angle between the radial vector from the origin of the  $x, z$  plane and the positive  $x$  axis.  $dz/dx = \tan \epsilon$  where  $\epsilon$  is the angle between the velocity vector projected onto the  $x, z$  plane and the positive  $x$ -axis. So, in this example,  $\tan \epsilon = \Lambda \tan \theta > \tan \theta$  and the flow vector is turned more toward the direction of the greater strain rate, i.e., the  $z$  direction here. (The inequality does not apply at  $\theta = 0, \pi/2, \pi$ , or  $3\pi/2$ .) In the hot zone,  $\Lambda$  has a larger value resulting in more turning there. In a constant-density case,  $\Lambda$  will be constant with  $y$ ; so, the streamline projection becomes identical for any  $x-z$  plane.

**V. 3D WALL STAGNATION-POINT FLOW**

For the wall stagnation flow, Eqs. (8), (10), (11), (27), and (28) still apply. The domain now is reduced to  $0 \leq \eta \leq \infty$ . The boundary conditions become

$$\begin{aligned}
 f_1'(\infty) = f_2'(\infty) = 1, \quad f_1'(0) = f_2'(0) = 0, \quad f_1(0) = f_2(0) = 0, \\
 v(\infty) = -(S_1 + S_2)\eta = -(S_1 + S_2)y, \quad v(0) = 0, \\
 h(\infty) = h_{\infty}, \quad h(0) = h_w.
 \end{aligned}
 \tag{41}$$

The solutions for  $v$  and  $p$  remain in the same form as given by Eqs. (8) and (27). While the forms for counterflow and wall stagnation flow are the same or similar, the changes in boundary conditions

for  $f_1$  and  $f_2$  due to the no-slip wall will affect the solutions.  $h_w$  is the gas enthalpy at the wall.

If  $\rho = 1$ ,  $\mu = 1$ , and  $\eta = y$ , we may obtain the solutions for the incompressible case. Howarth<sup>15</sup> has provided the incompressible steady solutions for the continuity and momentum equations but not for the energy equation.

Let us first examine the variable-density case where  $\rho\mu = 1$ . Then, the equations become

$$\begin{aligned}
 f_1'''' + (S_1 f_1 + S_2 f_2) f_1'' + S_1 [\tilde{h} - (f_1')^2] &= 0, \\
 f_2'''' + (S_1 f_1 + S_2 f_2) f_2'' + S_2 [\tilde{h} - (f_2')^2] &= 0, \\
 \tilde{h}'' + Pr(S_1 f_1 + S_2 f_2) \tilde{h}' &= 0, \\
 f_1'(\infty) = f_2'(\infty) = 1, \quad f_1'(0) = f_2'(0) = 0, \\
 f_1(0) = f_2(0) = 0, \quad \tilde{h}(\infty) = 1, \quad \tilde{h}(0) = \tilde{h}_w.
 \end{aligned}
 \tag{42}$$

In the above relation,  $\tilde{h}(\eta) \equiv h^*(\eta)/h^*(\infty)$  and the required constants are  $S_1, S_2 = 1 - S_1, \tilde{h}_w$ , and  $Pr$ . In the incompressible case,  $\tilde{h}$  in the first two ODEs above is replaced by 1, creating now only a one-way coupling with the third ODE for  $\tilde{h}$ .

Figures 10–12 give the computational wall-stagnation-flow results for various values of  $S_1, S_2, Pr$ , and  $\rho_w = h_{\infty}/h_w$ . Again, the rate of strain has modest effect on the scalar fields and  $v$ . Significant influence is seen on the  $u$  and  $w$  velocity components which

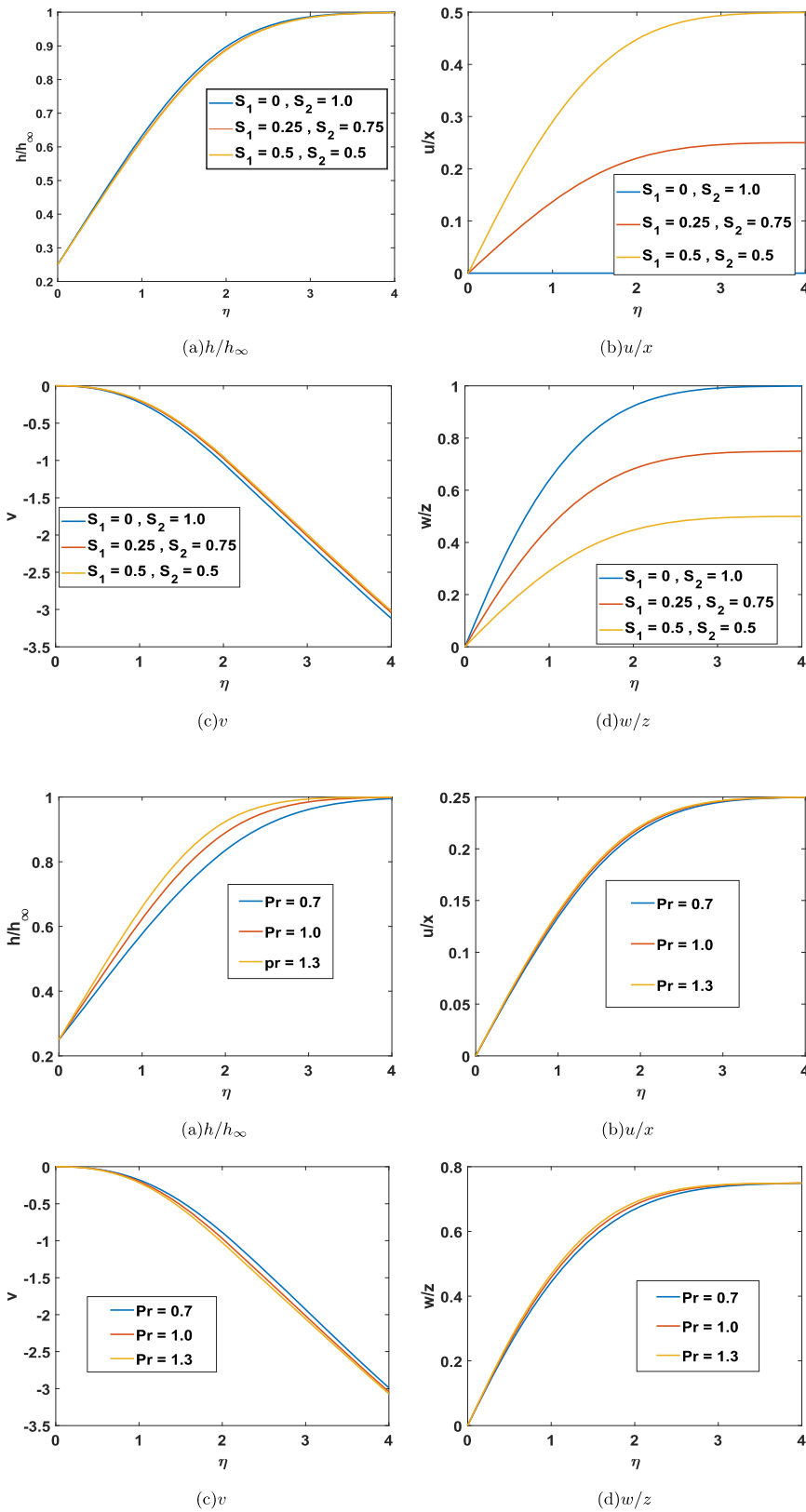


**FIG. 10.** Solutions for nondimensional velocities and enthalpy. Wall stagnation flow with various strain rate distributions.  $Pr = 1.0$  and  $h_w/h_\infty = 0.25$ .

**FIG. 11.** Solutions for nondimensional velocities and enthalpy. Wall stagnation flow with various Prandtl numbers.  $S_1 = 0.25$ ;  $S_2 = 0.75$ ;  $h_w/h_\infty = 0.25$ .

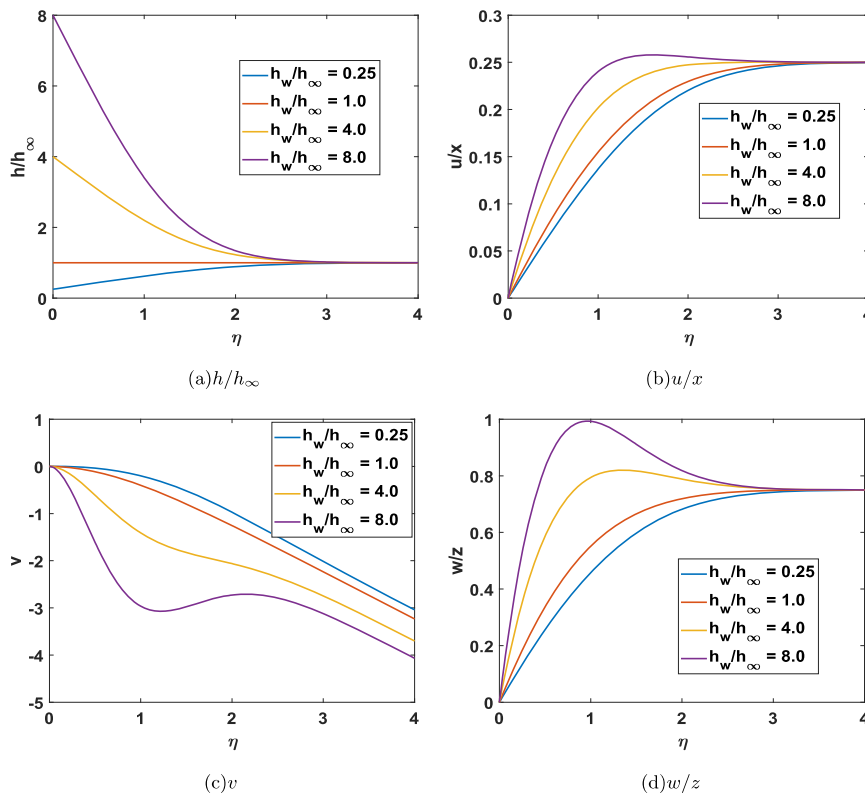


**FIG. 12.** Solutions for nondimensional velocities and enthalpy. Wall stagnation flow with various wall temperatures.  $S_1 = 0.25$ ;  $S_2 = 0.75$ ;  $Pr = 1.0$ .

each increases with normal strain values for their respective direction. The term  $S_{1,2}[\tilde{h} - (f'_{1,2})^2]$  in Eq. (31) can be large, especially near the wall. Still again, the results are readily extended since the values for  $u/x$ , and  $w/z$  can be interchanged with the values for  $w/z$  and  $u/x$  when  $S_1$  and  $S_2$  are replaced by  $1 - S_1$  and  $1 - S_2$ , respectively. For the case of a hot wall, Fig. 12 shows that all of the velocity components  $u$ ,  $v$ , and  $w$  have overshoots in the low-density region near that hot wall.

In similar fashion to the variable-density counterflow case, the extension of the results to a case with inflow from both the  $y$  and  $x$  (or  $z$ ) directions would not describe a plausible flow configuration.

## VI. CONCLUSIONS

Viscous counterflows and wall stagnation flows are analyzed with three-dimensional normal strain rates. Reacting (i.e., with diffusion flames) and nonreacting counterflows are examined. Stagnation flows with hot and cold walls are also studied. A similar system of the Navier-Stokes equations coupled with equations for scalar transport is developed, and exact solutions are obtained both inside and outside the viscous layer; i.e., the boundary-layer approximation is not required. The second derivatives of velocity go to zero outside of the viscous layer although first derivatives remain and asymptote to constants. Consequently, viscous force (per volume) asymptotes to zero and the Navier-Stokes equations asymptote to the Euler equations. Variable density, temperature, and composition are considered. Results for planar flows and axisymmetric flows are obtained as limits here. Velocity components  $u$ ,  $v$ , and  $w$  are each

odd functions of  $x$ ,  $y$ , and  $z$ , respectively. The scalar functions are even functions of both  $x$  and  $z$ . Terms of  $O(x^2, xz, z^2)$  are neglected.  $v(y)$  is determined for the infinite range of  $y$ .

For the steady and unsteady incompressible counterflows, analytical solutions are obtained for the flow field and the scalar fields subject to heat and mass transfer. In steady, variable-density configurations (both reacting and nonreacting), a set of ODEs govern the two transverse velocity profiles. Each of the three velocity components as well as the diffusion rates for mass, momentum, and energy depends on the two normal strain rates parallel to the counterflow interface or the wall and thereby not merely on the sum of those two strain rates. The effect of strain distribution is generally greater on the transverse velocity components,  $u$  and  $w$ , than on the incoming velocity component,  $v$ , and the scalar variables. The incompressible counterflow is the only case where the diffusion rate and the velocity component in the counterflow direction are not affected by the distribution of the strain rate between the two transverse directions and depend only on the sum of those two strain rates. The velocity profiles and the scalar profiles are shown to depend on ambient temperature (or equivalently density) values and the Prandtl number as well as the strain rates.

The results obtained here for both stagnation-point flows and counterflows agree exactly in the limits of two-dimensional flows (planar and axisymmetric) with the well known literature.<sup>1,6,13,14,17-19</sup> It also agrees with Howarth's results for three-dimensional, incompressible, steady wall-stagnation flow.<sup>15</sup>

The cited two-dimensional solutions and this new three-dimensional solution are exact solutions to the Navier-Stokes



equations for a region neighboring the stagnation point. For a flat interface of the opposing streams in counterflow or a flat wall in wall-stagnation flow, that neighborhood becomes infinite in size. Essentially, we have an acceptable solution if the ratio of the neighborhood size to the interface radius is much smaller than unity. Of course, improvements in the presentation here can be made by better representations of transport and physical property values, chemical kinetic descriptions, and in some cases equations of state.

For thin diffusion flames, the location, burning rate, and peak temperature are readily obtained in the infinite-kinetics limit. Important corrections are shown of the existing literature which is based on a constant-density assumption. For counterflows with flames and stagnation layers with hot walls, velocity overshoots are seen in the viscous layer for all three velocity components. The overshoot of velocity  $v$  in the incoming direction is driven by hot-gas expansion through the continuity equation. Then, for the turning flow, overshoots in the  $u$  and  $w$  velocity components also result. These overshoots also occur in the axisymmetric and planar limits although they were not recognized in prior studies on gaseous combustion.<sup>1,6,16–19</sup> The overshoot in the  $v$  velocity was presented for spray flames,<sup>20</sup> and, to a small extent, velocity overshoot appeared for combustion at supercritical pressure,<sup>22</sup> however without much discussion and no examination of the transverse velocity components. Here, solutions are found for a full range of the distribution of normal strain rates between the two transverse directions, various Prandtl number values, and various ambient (or wall) temperatures. The velocity overshoots for all three components show that large velocity gradients and vorticity of opposite directions are developing. These occurrences can have significant consequence for hydrodynamic stability and the development of turbulence. Also, it can add to the effect of flame stretch and subsequent extinction.

In steady counterflow and wall-stagnation flow, streamline projections on the  $x, y$  plane are the same for any  $z$  value. Similarly, projections on the  $y, z$  plane are the same for any  $x$  value. However, with variable density, projections onto an  $x, z$  plane will vary with  $y$ . A local reduction in density results in a local increase in the local strain-rate ratio beyond the ambient strain-rate ratio, thereby turning the flow vector locally even more in the direction of the greater strain rate.

Although viscous force goes to zero asymptotically with increasing distance from the wall or interface layer, the viscous dissipation rate asymptotes to a constant value.

## ACKNOWLEDGMENTS

This research was supported by the Air Force Office of Scientific Research under Grant No. FA9550-18-1-0392 with Dr. Mitat Birkan as the scientific officer. Information about existing literature from Professors D. Papamoschou, A. L. Sanchez, and F. A. Williams has been very helpful. The guidance from Professors T. Georgiou and A. Sideris on optimal use of Matlab for numerical integration is greatly appreciated.

## REFERENCES

- <sup>1</sup>A. Linan, "The asymptotic structure of counterflow diffusion flames for large activation energies," *Acta Astronaut.* **1**, 1007–1039 (1974).
- <sup>2</sup>F. E. Marble, "Growth of a diffusion flame in the field of a vortex," *Recent Advances in the Aerospace Sciences* (Plenum Press, New York, 1985), pp. 395–413.
- <sup>3</sup>A. R. Karagozian and F. E. Marble, "Study of a diffusion flame in a stretched vortex," *Combust. Sci. Technol.* **45**, 65–84 (1986).
- <sup>4</sup>B. M. Cetegen and W. A. Sirignano, "Study of molecular mixing and a finite rate chemical reaction in a mixing layer," *Symp. (Int.) Combust.* **22**, 489–494 (1988).
- <sup>5</sup>B. M. Cetegen and W. A. Sirignano, "Study of mixing and reaction in the field of a vortex," *Combust. Sci. Technol.* **72**, 157–181 (1990).
- <sup>6</sup>N. Peters, *Turbulent Combustion*, 1st ed. (Cambridge University Press, Cambridge, UK, 2000).
- <sup>7</sup>P. Rajamanickam, W. Coenen, A. L. Sanchez, and F. A. Williams, "Influences of stoichiometry on steadily propagating triple flames in counterflows," *Proc. Combust. Inst.* **37**, 1971–1977 (2019).
- <sup>8</sup>T. Nguyen, P. Popov, and W. A. Sirignano, "Longitudinal combustion instability in a rocket motor with a single coaxial injector," *J. Propul. Power* **34**(2), 354–373 (2018).
- <sup>9</sup>T. Nguyen and W. A. Sirignano, "The impacts of three flamelet burning regimes in nonlinear combustion dynamics, invited paper," *Combust. Flame* **195**, 170–182 (2018).
- <sup>10</sup>A. Bejan, "The concept of irreversibility in heat exchanger design: Counterflow heat exchangers for gas-to-gas applications," *J. Heat Transfer* **99**, 374–380 (1977).
- <sup>11</sup>V. N. Shtern and A. A. Borissov, "Counterflow driven by swirl decay," *Phys. Fluids* **22**, 063601 (2010).
- <sup>12</sup>T. V. Chagovets and S. W. Van Sciver, "A study of thermal counterflow using particle tracking velocimetry," *Phys. Fluids* **23**, 107102 (2011).
- <sup>13</sup>F. White, *Viscous Flows*, 3rd ed. (McGraw-Hill, 2005).
- <sup>14</sup>W. C. Strahle, "Periodic solutions to a convective droplet burning problem: The stagnation point," *Symp. (Int.) Combust.* **10**, 1315–1325 (1965).
- <sup>15</sup>L. Howarth, "CXLIV. The boundary layer in three dimensional flow. Part II. The flow near a stagnation point," *London, Edinburgh, Dublin Philos. Mag. J. Sci* **42**, 1433–1440 (1951).
- <sup>16</sup>M. D. Smooke, R. E. Mitchell, and M. E. Keyes, "Numerical solution of two-dimensional axisymmetric laminar diffusion flames," *Combust. Sci. Technol.* **67**, 85–122 (1986).
- <sup>17</sup>A. Linan, D. Martinez-Ruiz, M. Vera, and A. L. Sanchez, "The large-activation-energy analysis of extinction of counterflow diffusion flames with non-unity Lewis numbers of the fuel," *Combust. Flame* **175**, 91–106 (2017).
- <sup>18</sup>A. D. Weiss, M. Vera, A. Linan, A. L. Sanchez, and F. A. Williams, "A novel formulation for unsteady counterflow flames using a thermal-conductivity-weighted coordinate," *Combust. Theory Modell.* **22**, 185–201 (2018).
- <sup>19</sup>A. Linan and F. A. Williams, "Ignition in an unsteady mixing layer subject to strain and variable pressure," *Combust. Flame* **95**, 31–46 (1993).
- <sup>20</sup>G. Continillo and W. A. Sirignano, "Counterflow spray combustion modelling," *Combust. Flame* **81**, 325–340 (1990).
- <sup>21</sup>E. Gutheil and W. A. Sirignano, "Counterflow spray combustion modeling with detailed transport and detailed chemistry," *Combust. Flame* **113**, 92–105 (1998).
- <sup>22</sup>A. Jorda-Juanos and W. A. Sirignano, "Pressure effects on real-gas laminar counterflow," *Combust. Flame* **181**, 54–70 (2017).
- <sup>23</sup>A. D. Weiss, W. Coenen, and A. L. Sanchez, "Aerodynamics of planar counterflowing jets," *J. Fluid Mech.* **821**, 1–30 (2017).
- <sup>24</sup>J. Carpo, A. Linan, A. L. Sanchez, and F. A. Williams, "Aerodynamics of axisymmetric counterflowing jets," *Combust. Flame* **177**, 137–143 (2017).
- <sup>25</sup>Ya. B. Zel'dovich and Yu. P. Raizer, *Physics of Shock Waves and High-Temperature Hydrodynamic Phenomena* (Dover, Mineola, N.Y., 2002).
- <sup>26</sup>R. W. Bilger, "The structure of diffusion flames," *Combust. Sci. Technol.* **13**, 155–170 (1976).